CHAPTER VII

APPLICATIONS TO PROBLEMS IN POLYMER PHYSICS AND RHEOLOGY

H. SCHIESSEL
Theoretical Polymer Physics, Freiburg University, Rheinstr. 12, 79104 Freiburg, Germany and Materials Research Laboratory, University of California, Santa Barbara, CA 93106-5130, USA

CHR. FRIEDRICH
Freiburg Materials' Research Center, Freiburg University, Stefan-Meier-Str. 21, 70104 Freiburg, Germany

A. BLUMEN
Theoretical Polymer Physics, Freiburg University, Rheinstr. 12, 79104 Freiburg, Germany

Contents

1 Introduction

Power law relaxation is of widespread occurrence in complex materials. Thus one often encounters algebraic relaxation functions

$$\Phi(t) \propto t^{-\alpha} \tag{1}$$

with $0 < \alpha < 1$. Examples are the transport of charge carriers in amorphous semiconductors [1,2], the behavior of electrical currents at rough blocking electrodes [3], the dielectric relaxation of liquids [4] and of solids [5] and the attenuation of seismic waves [6]. Especially the microscopic and macroscopic dynamical behavior of macromolecular systems (such as linear polymers or gels) is often characterized by the algebraic patterns of Eq. (1) [7].

For such systems fractional expressions come naturally into play as a result of the superposition principle. Consider an arbitrary history of the external perturbation $\Psi(t)$, and let us denote by $\Phi_s(t)$ the response of the system to steplike external perturbations $\Psi(t) = \Theta(t)$, where $\Theta(t)$ is the Heaviside step function. Then we obtain the response of the system by the causal convolution:

$$\Phi(t) = \int_{-\infty}^{t} dt' \Phi_s(t - t') \frac{d\Psi(t')}{dt'} \tag{2}$$

since the (Boltzmann) superposition integral, Eq. (2), holds for linear systems which are homogeneous in time. Specifically, let Φ_s obey:

$$\Phi_s(t) = \frac{C}{\Gamma(1-\alpha)} \left(\frac{t}{\tau}\right)^{-\alpha}, \tag{3}$$

where $\Gamma(x)$ denotes the Gamma function. Eq. (3) is chosen in such a way as to match the forthcoming definitions. Now we find the response $\Phi(t)$ to an arbitrary $\Psi(t)$ by inserting Eq. (3) into Eq. (2):

$$\Phi(t) = \frac{C\tau^{\alpha}}{\Gamma(1-\alpha)} \int_{-\infty}^{t} dt' (t - t')^{-\alpha} \frac{d\Psi(t')}{dt'}. \tag{4}$$

The right-hand-side of Eq. (4) is nothing but a fractional integral. This is most readily seen by recalling the definition of Riemann's fractional integral [8,9]:

$${}_cD_t^{-\gamma} f(t) = \frac{1}{\Gamma(\gamma)} \int_{c}^{t} dt' \frac{f(t')}{(t - t')^{1-\gamma}}, \tag{5}$$

where $\gamma > 0$. Equation (5) embraces two special cases: (*i*) The case $c = 0$ corresponds to a fractional integral of Riemann-Liouville type. (*ii*) $c \to -\infty$ leads to Weyl's version of fractional calculus. Fractional differentiation of order $\gamma > 0$ is now obtained by first picking an integer n, $n > \gamma$, then performing a fractional integration of order $n - \gamma$, followed by an ordinary differentiation of order n, i.e.

$$ {}_cD_t^{\gamma} f(t) = \frac{d^n}{dt^n} \left[{}_cD_t^{\gamma - n} f(t) \right]. \tag{6} $$

We work in the following within Weyl's formalism, i.e. $c \to -\infty$, and use the shorthand notation $d^{\gamma}/dt^{\gamma} \equiv {}_{-\infty}D_t^{\gamma}$. In Weyl's version the composition rule for differentiation and integration obeys the simple form

$$ \frac{d^{\alpha}}{dt^{\alpha}} \frac{d^{\beta}}{dt^{\beta}} = \frac{d^{\alpha+\beta}}{dt^{\alpha+\beta}} \tag{7} $$

for arbitrary α and β [9].

Using Eqs. (5) to (7) we can rewrite the causal convolution, Eq. (4) as:

$$ \Phi(t) = C\tau^{\alpha} \frac{d^{\alpha-1}}{dt^{\alpha-1}} \frac{d\Psi(t)}{dt} = C\tau^{\alpha} \frac{d^{\alpha}\Psi(t)}{dt^{\alpha}}. \tag{8} $$

Thus we find that here the system's response, $\Phi(t)$, follows by the fractional differentiation of the external perturbation, $\Psi(t)$.

We consider now the same system, but exchange the roles of Φ and Ψ, *i.e.*, view Ψ as being the response to a prescribed Φ. Such a reversal can be achieved experimentally for systems in which both quantities can be controlled (for instance, the stress and the strain in a rheological experiment). In order to find the corresponding fractional expression we have simply to apply the fractional operator $d^{-\alpha}/dt^{-\alpha}$ to both sides of Eq. (8), which leads to

$$ \Psi(t) = C^{-1}\tau^{-\alpha} \frac{d^{-\alpha}\Phi(t)}{dt^{-\alpha}}. \tag{9} $$

By rewriting Eq. (9) as

$$ \Psi(t) = C^{-1}\tau^{-\alpha} \frac{d^{-\alpha-1}}{dt^{-\alpha-1}} \frac{d\Phi}{dt} = \frac{C^{-1}\tau^{-\alpha}}{\Gamma(1+\alpha)} \int_{-\infty}^{t} dt' \, (t-t')^{\alpha} \frac{d\Phi(t')}{dt'} \tag{10} $$

we can infer immediately that the response Ψ_s to a steplike perturbation $\Phi(t) = \Theta(t)$ is

$$ \Psi_s(t) = \frac{C^{-1}}{\Gamma(1+\alpha)} \left(\frac{t}{\tau} \right)^{\alpha} \tag{11} $$

2 Applications to Microscopic Models of Polymer Dynamics

Macromolecular systems show in many cases viscoelastic behavior, which combines the characteristic features of solids (elasticity) and of liquids (viscosity). Traditional rheological methods measure the materials' properties at large length scales, and we will discuss applications of fractional calculus to this class of experiments in Sec. 3. Recent optical developments allow, however, the micromanipulation of macromolecules so that one has means at hand to measure local mechanical properties. Thus Perkins et al. [10]–[12] and Wirtz [13] have dragged individual fluorescent DNAs with optical or magnetic tweezers at one end; Amblard et al. [14] have performed similar experiments with individual magnetic beads in actin networks. In this section we focus on such a class of experiments on polymer chains and networks. We prefer here not to take all experimentally relevant factors into account, such as the excluded volume, the finite extensibility, the bending rigidity, the hydrodynamic coupling (such effects were discussed, for instance, in Refs. [14]–[17]), but to focus on the rather simple Rouse model for polymer dynamics [18,19]. Thus, using the Rouse model we demonstrate how, as a result of the superposition principle (or equivalently of simple scaling relations) fractional expressions such as Eq. (9) come into play, and we determine the local dynamics of polymer chains and networks.

2.1 Pulling a Rouse Chain at One of its Ends

In the following we show how a prototype model of polymer dynamics, the Rouse model [18,19], leads rigorously to a fractional differential equation of the form of Eq. (9). We demonstrate this for an external force which acts on one end-monomer of the chain.

The polymer is modeled as a Gaussian chain consisting of N monomers, connected by harmonic springs to a linear chain. The chain's configuration is given by the set of vectors $\{\mathbf{R}_n(t)\}$, where $\mathbf{R}_n(t) = (X_n(t), Y_n(t), Z_n(t))$ is the position vector of the nth bead at time t, $n = 0, 1, \ldots N-1$. The potential energy $U(\{\mathbf{R}_n(t)\})$ has to account for the elastic contributions and for the influence of the external force $\mathbf{F}(t)$, which is assumed to act on the monomer $n = 0$. Thus one has

$$U(\{\mathbf{R}_n(t)\}) = \frac{K}{2}\sum_{n=1}^{N-1}\left[\mathbf{R}_n(t) - \mathbf{R}_{n-1}(t)\right]^2 - \mathbf{F}(t)\,\mathbf{R}_0(t)\,. \tag{12}$$

In Eq. (12) K is the (entropic) spring constant $K = 3T/b^2$, where T denotes the

temperature in units of the Boltzmann constant k_B, and b is the mean distance between neighboring beads (in the absence of an external perturbation). The chain's dynamics is described by N coupled Langevin equations [18,19]

$$\zeta \frac{d\mathbf{R}_n(t)}{dt} = -\frac{\partial U(\{\mathbf{R}_n(t)\})}{\partial \mathbf{R}_n(t)} + \mathbf{f}_R(n,t) \tag{13}$$

and the hydrodynamic interaction between the beads is disregarded. In Eq. (13) ζ is the friction constant and $\mathbf{f}_R(n,t)$ is the random thermal-noise force which mimics the collisions of the nth bead of the chain with the solvent molecules. The thermal noise is Gaussian, white, with zero mean, so that one has:

$$\overline{f_i(n,t)} = 0,\ \overline{f_i(n,t) f_j(n',t')} = 2\zeta T \delta_{ij} \delta_{nn'} \delta(t-t'). \tag{14}$$

In Eq. (14) i and j denote the components of the force vector, i.e. $i,j = X,Y,Z$ and the overbar stands for thermal averaging, i.e. averaging over the realizations of the Langevin forces $\mathbf{f}_R(n,t)$.

Taking the variable n to be continuous (i.e. considering the chain as an elastic string) and setting $\mathbf{F}(t) = (0, F(t), 0)$, it follows from Eqs. (12) and (13) that:

$$\zeta \frac{\partial X_n(t)}{\partial t} = K \frac{\partial^2 X_n(t)}{\partial n^2} + f_X(n,t), \tag{15}$$

$$\zeta \frac{\partial Z_n(t)}{\partial t} = K \frac{\partial^2 Z_n(t)}{\partial n^2} + f_Z(n,t) \tag{16}$$

and

$$\zeta \frac{\partial Y_n(t)}{\partial t} = K \frac{\partial^2 Y_n(t)}{\partial n^2} + \delta_{n0} F(t) + f_Y(n,t). \tag{17}$$

At the chain's ends the Rouse boundary conditions [18,19] hold:

$$\left.\frac{\partial X_n(t)}{\partial n}\right|_{n=0,N} = \left.\frac{\partial Y_n(t)}{\partial n}\right|_{n=0,N} = \left.\frac{\partial Z_n(t)}{\partial n}\right|_{n=0,N} = 0. \tag{18}$$

Since the X- and Z-components of the $\mathbf{R}_n$ are force-independent and follow the standard Rouse behavior [18,19] we can restrict ourselves to the behavior of the Y-component, Eq. (17). This equation contains two types of forces: the thermal noise term $f_Y(n,t)$ and the external force $F(t)$ which acts on the first monomer.

The solution of Eq. (17) with the boundary conditions, Eq. (18), can be given in the form of a Fourier series [19]

$$Y_n(t) = Y(0,t) + 2\sum_{p=1}^{\infty} Y(p,t)\cos\left(\frac{p\pi n}{N}\right) \tag{19}$$

where $Y(p,t)$, $p = 0, 1, ...$, denote the normal coordinates:

$$Y(p,t) = \frac{1}{N}\int_0^N dn \cos\left(\frac{p\pi n}{N}\right) Y_n(t). \tag{20}$$

In terms of the coordinates $Y(p,t)$ Eq. (17) can be rewritten as

$$\frac{\partial Y(p,t)}{\partial t} = -\frac{p^2}{\tau_R} Y(p,t) + \frac{1}{N\zeta} F(t) + \frac{1}{\zeta}\varphi_Y(p,t). \tag{21}$$

Here τ_R denotes the Rouse time

$$\tau_R = \frac{\zeta b^2 N^2}{3\pi^2 T} \tag{22}$$

which is the longest internal relaxation time of the harmonic chain. The symbol $\varphi_Y(p,t)$ in Eq. (21) denotes the Fourier transform of the thermal noises $\varphi_Y(p,t) = N^{-1}\int_0^N dn \cos(p\pi n/N) f_Y(n,t)$.

We assume that the chain is at $t = 0$ in thermal equilibrium, i.e. it has a Gaussian conformation. This can be accounted for automatically by stipulating the polymer to have been subjected to the thermal forces since $t = -\infty$. Furthermore, switching on the external force at $t = 0$, i.e. having $F(t) = F_0\Theta(t)$, the normal coordinates are given by

$$\begin{aligned} Y(p,t) &= \frac{1}{\zeta}\int_{-\infty}^{t} d\tau \varphi_Y(p,\tau)\exp\left(-p^2(t-\tau)/\tau_R\right) \\ &\quad + \frac{F_0}{N\zeta}\int_0^t d\tau \exp\left(-p^2(t-\tau)/\tau_R\right). \end{aligned} \tag{23}$$

From Eqs. (19) and (23) one can obtain readily the explicit time dependence of several different quantities such as the end-to-end distance, the displacement of the chain's center of mass (CM), or that of a tagged bead (cf. for instance Refs. [20,21]).

Consider first the CM's motion. The Y-component of the trajectory of the CM is given by the 0th normal coordinate, i.e. by $Y_{CM}(t) = N^{-1}\int_0^N dn Y_n(t) = Y(0,t)$. Using Eq. (23) with $p = 0$ we find for the mean averaged position of the chain's CM in the Y-direction:

$$\overline{Y_{CM}(t)} = \frac{F_0}{N\zeta}t \tag{24}$$

i.e., the chain drifts with a constant velocity $F_0/N\zeta$. From Eq. (24) one can infer that the friction constant of the overall chain is $N\zeta$, which is the sum of the friction constants of the individual monomers: Due to the neglect of hydrodynamic interactions in Eq. (13), the Rouse chain is free draining.

The behavior of a tagged bead, say one of the chain's ends, is more complicated. Using Eq. (19) with $n = 0$, i.e.

$$Y_0(t) = Y(0,t) + 2\sum_{p=1}^{\infty} Y(p,t) \tag{25}$$

we obtain from Eqs. (23) and (25) for the MSD of the 0th bead

$$\overline{Y_0(t)} = \frac{F_0}{N\zeta}t + \frac{2F_0}{N\zeta}\sum_{p=1}^{\infty}\int_0^t d\tau \exp\left(-p^2\tau/\tau_R\right) . \tag{26}$$

From Eq. (26) the short-time behavior, $t \ll \tau_R$, follows by converting the sum over p into an integral; this leads to:

$$\overline{Y_0(t)} \cong \frac{2bF_0}{\sqrt{3\pi\zeta T}}t^{1/2} = \frac{2}{\sqrt{\pi}}\frac{F_0}{\sqrt{\zeta K}}t^{1/2}. \tag{27}$$

In Eq. (27) we have omitted the first term on the rhs of Eq. (26), which is of the order of $\sqrt{t/\tau_R}$ smaller than the second term. In the long time regime $t \gg \tau_R$ one finds the second term of Eq. (26) to be of the order of τ_R/t smaller than the first one. Thus one has

$$\overline{Y_0(t)} \cong \frac{F_0}{N\zeta}t, \tag{28}$$

i.e. the bead's motion mirrors the motion of the CM of the chain, Eq. (24).

Now Eq. (27) is a nice example which shows how fractional relationships come into play in polymer dynamics. Assume the chain to very long, $N \gg 1$; since the Rouse time obeys $\tau_R \propto N^2$, the range of validity of Eq. (27)

becomes very large. One may even consider the limit $N \to \infty$, where Eq. (27) becomes exact for all positive times. Assume now an arbitrary history $F(t)$ of the external force. Then, due to the linearity of the system one finds the convolution integral

$$\overline{Y_0(t)} = \frac{1}{\sqrt{\zeta K}} \frac{1}{\Gamma(3/2)} \int_{-\infty}^{t} \frac{d\tau}{(t-\tau)^{1-3/2}} \frac{dF(\tau)}{d\tau} = \frac{1}{\sqrt{\zeta K}} \frac{d^{-3/2}}{dt^{-3/2}} \left[\frac{dF(t)}{dt}\right] \quad (29)$$

which represents Weyl's integral (cf. Eq. (5) with $c \to \infty$). Using the composition rule, Eq. (7), leads finally to:

$$\overline{Y_0(t)} = \frac{1}{\sqrt{\zeta K}} \frac{d^{-1/2} F(t)}{dt^{-1/2}}. \quad (30)$$

Thus the mean position of bead $n = 0$ (which is subjected to the external force) follows from the semiintegration of the force history $F(t)$.

We close this section by showing how Eq. (27) can also be derived using scaling arguments. Consider the tagged bead $n = 0$. After switching on the force at $t = 0$, the number $g(t)$ of monomers which move together with the tagged bead increases with t. This number follows from the Rouse time associated with a subchain of g monomers, namely from $\tau_g \approx \zeta b^2 g^2 / T$. Inverting this relation leads to:

$$g(t) \approx \frac{\sqrt{T}}{\sqrt{\zeta} b} t^{1/2}. \quad (31)$$

Eq. (31) describes the short time behavior, $t \ll \tau_R$, whereas at longer times, $t \gg \tau_R$, one has

$$g(t) \cong N, \quad (32)$$

i.e. the whole chain moves collectively. The mobility of the set of g beads decreases with time as $\mu(t) \cong (\zeta g(t))^{-1}$. The average velocity v_Y in the Y-direction of the tagged monomer is given by the velocity of the set of monomers moving together with it; hence $v_Y(t) = \mu(t) F_0 = (\zeta g(t))^{-1} F_0$, where g is given by Eq. (31) for $t \ll \tau_R$ and by Eq. (32) for $t \gg \tau_R$. The average displacement of a single bead can be estimated from the average displacement of the corresponding blob of g monomers, i.e. $\overline{Y_0(t)} = v_Y(t)\, t = (\zeta g(t))^{-1} F_0 t$. For $t \ll \tau_R$ one finds from Eq. (31)

$$\overline{Y_0(t)} \approx \frac{b F_0}{\sqrt{\zeta T}} t^{1/2}, \quad (33)$$

i.e., we recover (up to numerical coefficients of order unity) Eq. (27), the result of the previous, exact calculations. For longer times the PA drifts as a whole, and we find from Eq. (32) $\overline{Y_0(t)} \approx (N\zeta)^{-1} F_0 t$, which corresponds to Eq. (28).

In Sec. 2.2 we will discuss how Eq. (30) can be generalized to an arbitrary order α of integration, with α obeying $0 < \alpha \leq 1/2$. This is achieved by pulling a monomer which belongs to a branched structure (fractal network); then α is directly related to the connectivity of the network.

2.2 Pulling One Monomer of a Fractal Network

Consider again the scaling arguments which led us to Eq. (33). The $t^{1/2}$-subdrift displacement follows from the increase in the number $g(t) \propto t^{1/2}$ of monomers which are moving collectively: this slows down the tagged bead. It is evident that pulling a monomer of a macromolecular network (which is more tight than a linear chain) involves an even slower subdrift. Examples of such networks are the *generalized Gaussian structures* (GGS), which were considered by Sommer and Blumen [22]. We investigate here some of the dynamical properties of such GGS, especially isotropic and locally homogeneous fractals, which may be seen as prototypes for membranes, gels and polymer networks.

In order to obtain $g(t)$ for the GGS it is useful to rederive Eqs. (31) and (32) in a slightly different way. Note that Rouse dynamics leads to Eq. (17) which is a one-dimensional equation of diffusion-type. As it is well-known, its Green's function is a Gaussian, whose width increases with time as $t^{1/2}$; stated differently, the number of monomers $g(t)$ which are involved in a collective motion obeys $g(t) \propto t^{1/2}$.

Consider now the Rouse dynamics of a fractal GGS. This leads to a diffusion equation on the corresponding fractal lattice. It is well-known that the number $S(t)$ of different sites visited by a random walker during time t goes as $S(t) \propto t^{d_s/2}$ for $d_s < 2$ and as $S(t) \propto t$ for $d_s \geq 2$. Here d_s denotes the spectral dimension of the network (see, for instance, Refs. [23,24]); in the case of a regular lattice d_s equals the Euclidian dimension. Now, the dynamical process has a single parameter combination with the dimension of time, namely $\zeta b^2/T$; we thus find:

$$g(t) \approx \begin{cases} \frac{T^{d_s/2}}{\zeta^{d_s/2} b^{d_s}} t^{d_s/2} & \text{for } d_s < 2 \\ \frac{T}{\zeta b^2} t & \text{for } d_s \geq 2. \end{cases} \tag{34}$$

Eq. (34) is valid as long as the network does not move as a whole; at later times $g(t) = N$ holds. The crossover time τ_G follows by setting $g(\tau_G) = N$ in

Eq. (34). For $d_s < 2$ this leads to

$$\tau_G \approx \zeta b^2 N^{2/d_s}/T. \tag{35}$$

For a linear chain, $d_s = 1$, one recovers the Rouse time, Eq. (22). We proceed now as in Sec. 2.1. The domain which moves collectively has the velocity $v_Y(t) = (\zeta g(t))^{-1} F_0$. For $d_s < 2$ this leads to the following displacement of the tagged monomer

$$\overline{Y(t)} \approx \frac{F_0 b^{d_s}}{\zeta^{1-d_s/2} T^{d_s/2}} t^{1-d_s/2}. \tag{36}$$

The displacement due to an arbitrary force $F(t)$ is thus given by

$$\overline{Y(t)} \approx \frac{b^{d_s}}{\zeta^{1-d_s/2} T^{d_s/2}} \frac{d^{d_s/2-1} F(t)}{dt^{d_s/2-1}}. \tag{37}$$

Thus we have suceeded in deriving an expression with a fractional integral of order $\alpha = 1 - d_s/2$, where $0 < \alpha \leq 1/2$.

We close this section with a short discussion of the case $d_s \geq 2$. Sommer and Blumen [22] showed that the corresponding GGS (without an external force) is then in a collapsed state. Using a Langevin-type approach Schiessel [25] showed that in this case one has a very weak time-dependence of $\overline{Y(t)}$, which results from the fact that the external force is unable to unfold the collapsed structure. In Sec. 2.4 we show how more general perturbations which act on the whole GGS are able to unfold structures whose spectral dimensions are less than 4.

2.3 Polyampholytes in External Electrical Fields

We turn now to the dynamics of polyampholytes (PAs) in external electrical fields. This allows us to obtain relations similar to Eq. (30), with orders of integration α within the range $1/2 \leq \alpha \leq 1$. PAs are heteropolymers carrying positive and negative charges along their backbone, forming quenched (random or regular) patterns. The conformational and dynamical properties of PAs show interesting features: (*i*) The interactions between the different positive and negative charges lead in many cases to the collapse of the chains into spherical globules [26,27]. (*ii*) For PAs with a sufficiently high total charge the globular state is not stable; one has then a random necklace structure with globular and stretched parts [28,29]. (*iii*) In a sufficiently strong external field a PA globule is unstable and stretches out [29]– [32].

This plethora of static (conformational) features has its counterpart in the dynamics, and the situation is very complex. Here we restrict the analysis to an

important, limiting case, namely to the weak coupling limit (WCL), in which the interaction between the charges can be neglected and where the behavior of PAs in external fields can be handled with some ease [20] [21] [29] [36]. This WCL can be realized through weakly charged PAs. As an example consider a PA with N monomers, with fN positive $(+q)$ and fN negative $(-q)$ charges, randomly distributed along the backbone of the chain; $f \leq 1/2$ denotes the fraction of positively (as well as negatively) charged monomers. In this case the interaction between the charges can be neglected if $b > N^{1/2} f l_B$, where $l_B = q^2/(\varepsilon T)$ denotes the Bjerrum length and ε the dielectric constant [26,27,31,32]; in water at room temperature one has $l_B \approx 7\text{Å}$.

We now follow Refs. [20,21] and model, similar to Sec. 2.1, the PA as a Rouse chain. We denote the charge on the nth bead by q_n and take it to be a quenched variable, *i.e.*, the set $\{q_n\}$ stays fixed for a given PA. The potential $U(\{\mathbf{R}_n(t)\})$ in an external electrical field $\mathbf{E}$ is then given by

$$U(\{\mathbf{R}_n(t)\}) = \frac{K}{2} \sum_{n=1}^{N-1} [\mathbf{R}_n(t) - \mathbf{R}_{n-1}(t)]^2 - \mathbf{E} \sum_{n=1}^{N-1} q_n \mathbf{R}_n(t) . \tag{38}$$

In order to calculate the dynamics of the PA one can now follow Sec. 2.1. The equations of motion are given by Eq. (13) which again decouples in Cartesian coordinates. For $\mathbf{E} = (0, E, 0)$ this leads to Eqs. (15) and (16) for the X- and the Z-component, whereas the dynamics in field direction is given by

$$\zeta \frac{\partial Y_n(t)}{\partial t} = K \frac{\partial^2 Y_n(t)}{\partial n^2} + q_n E + f_Y(n,t) . \tag{39}$$

By transforming to Rouse normal coordinates (as in Sec. 2.1) one can readily evaluate several PA properties for different charge distributions $\{q_n\}$: see Ref. [21] for an explicit calculation of the position of the CM, of that of particular beads, as well as for the evaluation of the PA's end-to-end distance. We dispense here with giving the explicit derivation of the formulas and only present a result which again leads to a fractional expression.

Consider a PA with a random, uncorrelated charge distribution, *i.e.* $\langle q_n q_m \rangle = q^2 \delta_{nm}$ (the brackets denote the average with respect to different $\{q_n\}$ realisations). At short times, $t \ll \tau_R$, and neglecting the thermal contributions, the mean-squared displacement of bead $n = 0$ obeys:

$$\left\langle \left(\overline{Y_0(t)} \right)^2 \right\rangle = \frac{8bq^2E^2\left(\sqrt{2}-1\right)}{3\zeta^{3/2}\sqrt{3\pi T}} t^{3/2} \tag{40}$$

(see Refs. [20,21] for the full expression). Hence, from Eq. (40) the mean-squared displacement of the bead follows a $t^{3/2}$-subdrift behavior. On the

other hand for $t \gg \tau_R$ (and again neglecting the thermal contributions) one has

$$\left\langle \left(\overline{Y_0(t)}\right)^2 \right\rangle = \frac{q^2 E^2}{\zeta^2 N} t^2. \tag{41}$$

Here the displacement of the tagged bead mirrors the CM's motion (note that the average total charge is of the order of $q\sqrt{N}$).

Eq. (40) is again an example of a power law: After switching on the field, the displacement of the zeroth bead is given by $\widehat{Y}_0(t) \approx \left(b^{1/2} qE/\zeta^{3/4} T^{1/4}\right) t^{3/4}$, as long as $t < \tau_R$; here the hat denotes the averaging procedure $\widehat{f}(t) = \left\langle \left(\overline{f(t)}\right)^2 \right\rangle^{1/2}$. For large N the Rouse-time τ_R is very large ($\tau_R \propto N^2$) and one has

$$\widehat{Y}_0(t) \approx \frac{b^{1/2} q}{\zeta^{3/4} T^{1/4}} \int_{-\infty}^{t} \frac{d\tau}{(t-\tau)^{1-7/4}} \frac{dE(\tau)}{d\tau} \approx \frac{b^{1/2} q}{\zeta^{3/4} T^{1/4}} \frac{d^{-3/4} E(t)}{dt^{-3/4}}, \tag{42}$$

i.e., for an arbitrary history of the electrical field $E(t)$ the displacement of the bead is given by a fractional integration of $E(t)$ of order 3/4.

What leads to an exponent of 3/4? And can the exponent also assume other values? To clarify this we apply scaling arguments (as in Sec. 2.1) to PAs with random, uncorrelated charge distributions. In the following we consider general charge patterns, namely random, long-range correlated sequences of charges [31]. For such sequences the net charge of the PA is given by $\langle Q_{tot}^2 \rangle \cong q^2 N^{2\gamma}$ with $0 \leq \gamma \leq 1$. The case $\gamma = 1/2$ corresponds to the uncorrelated distribution discussed above, whereas for $\gamma > 1/2$ the charges are positively, and for $\gamma < 1/2$ negatively correlated. The extreme cases $\gamma = 1$ and $\gamma = 0$ are realized by polyelectrolytes ($q_n \equiv q$ or $q_n \equiv -q$) and by alternating PAs ($q_n = (-1)^n q$), respectively.

Consider now a single bead. We know from Sec. 2.1 the short- and long-time behavior of the total number g of neighboring monomers which are involved in a collective motion with this tagged bead (cf. Eqs. (31) and (32)). The excess charge Q of this collectively moving set of beads grows with time as $\langle Q^2 \rangle \cong q^2 (g(t))^{2\gamma}$, whereas its mobility decreases with time as $\mu \cong (\zeta g(t))^{-1}$. The average velocity of the tagged monomer in the Y-direction, v_Y, equals the velocity of the collectively moving set around it. Hence $\widehat{v}_Y^2(g) \cong \mu^2 \langle Q^2 \rangle E^2 \cong q^2 E^2 \zeta^{-2} g^{2\gamma-2}$, where g is given by Eq. (31) for $t \ll \tau_R$ and by Eq. (32) for $t \gg \tau_R$. The average displacement $\widehat{Y}(t)$ of a single bead, follows from the average displacement of the corresponding group

of g neighbors, *i.e.* $\widehat{Y}^2(t) \cong \widehat{v}_Y^2(g)\, t^2 \cong q^2E^2\zeta^{-2}g^{2\gamma-2}t^2$. For $t \ll \tau_R$ one finds from Eq. (31)

$$\widehat{Y}^2(t) \cong \frac{b^{2-2\gamma}q^2E^2}{\zeta^{1+\gamma}T^{1-\gamma}}t^{1+\gamma}. \tag{43}$$

For the uncorrelated case, $\gamma = 1/2$, this reproduces (up to a numerical constant of order unity) the field induced short-time behavior of the exact calculations, *i.e.* Eq. (40). At longer times the PA drifts as a whole, and from Eq. (32) we find that $\widehat{Y}^2(t) \cong \left(q^2E^2/\zeta^2N^{2-2\gamma}\right)t^2$, which for $\gamma = 1/2$ reproduces Eq. (41). Note that for polyelectrolytes, $\gamma = 1$, the drift becomes independent of N.

With Eq. (43) we have found a power law of the form $\widehat{Y}(t) \propto t^{(1+\gamma)/2}$, which leads us to a generalization of the fractional relationships Eqs. (30) and (42), namely to:

$$\widehat{Y}(t) \approx \frac{b^{1-\gamma}q}{\zeta^{(1+\gamma)/2}T^{(1-\gamma)/2}} \frac{d^{-(1+\gamma)/2}E(t)}{dt^{-(1+\gamma)/2}} \ . \tag{44}$$

In Eq. (44) the order of integration ranges from 1/2 (alternating case) to 1 (polyelectrolyte).

2.4 Polyampholytic Networks in External Electrical Fields

Consider a GGS where each monomer carries a charge, so that $q_n = \pm q$. Assume that the charges are distributed in such a way that $\langle Q_{tot}^2 \rangle \cong q^2N^{2\gamma}$. Note that the cases $\gamma = 1/2$ and $\gamma = 1$ can be simply realized, whereas long-ranged (anti)correlations cannot be simply induced for many non-trivial connectivities. Using Eq. (34) one finds with $\widehat{v}_Y = QE/(g\zeta) \approx qE/\left(g^{1-\gamma}\zeta\right)$ for $d_s < 2$:

$$\widehat{Y}(t) \approx \left(\zeta b^2/T\right)^{(1-\gamma)d_s/2} \frac{qE}{\zeta} t^{1-(1-\gamma)d_s/2}. \tag{45}$$

The equilibrium value of the typical size R of the PA in the external field is reached at τ_G; one has for $\gamma = 1/2$

$$R \approx \widehat{Y}(\tau_G) \approx \frac{b^2qE}{T}N^{(4-d_s)/(2d_s)}, \tag{46}$$

a relation which was derived by Sommer and Blumen [22].

Interestingly, the range of validity of Eq. (45) extends – depending on the value γ – to larger d_s-values. Consider, for instance, the uncorrelated case $\gamma = 1/2$. Then the exponent of t, namely $1-(1-\gamma)\,d_s/2$ is positive as long as

$d_s < 4$. One can show using more refined arguments [25] that here Eqs. (45) and (46) remain indeed valid also for $2 < d_s < 4$. Note, however, that for $d_s > 2\ g(t)$, Eq. (34), is independent of d_s, so that our simplified argument does not work here.

This example shows that the interplay between the connectivity of the network and the charge distribution is not in every case multiplicative, *i.e.* does not subordinate (cf. the similar phenomenon discussed in Ref. [37]). In order to obtain the exponents for all d_s- and γ-values one is forced to use a more detailed analysis, which is given in Ref. [25].

We close by giving the corresponding fractional relation for an arbitrary time-dependence of $E(t)$:

$$\widehat{Y}(t) \approx \left(\zeta b^2/T\right)^{(1-\gamma)d_s/2} \frac{q}{\zeta} \frac{d^{(1-\gamma)d_s/2-1} E(t)}{dt^{(1-\gamma)d_s/2-1}}, \tag{47}$$

a relation which generalizes the fractional Eqs. (37) and (44). The order of integration extends now from 0 to -1; note, however, that Eq. (47) is only valid for sufficiently small d_s-values, namely $d_s < 2/(1-\gamma)$ [25].

2.5 Rouse Dynamics of Generalized Gaussian Structures: Connection to Macroscopic Properties

Until now we have considered the local dynamical properties of Rouse chains and of GGSs; now one may raise the question in how far the local dynamics influence the macroscopic properties of, say, a solution of GGSs. We will show in this section that the microscopic dynamics also determine the macroscopic viscoelastic properties of a GGS-solution; thus fractional force-displacement relationships translate into fractional stress-strain relationships of the whole sample.

We follow here the general treatment of viscoelasticity for polymer solutions, for suspensions etc. which is given in chapter 3.7 of Ref. [19] and apply it to GGS solutions. Let us assume to have a solution of identical GGSs and denote with c the concentration of the monomers, *i.e.* c/N is the concentration of the GGSs. The problem is now to find a microscopic expression for the stress tensor $\sigma_{\alpha\beta}$, say for the component σ_{zx} (for its definition cf. Ref. [38,39]). To this end let us consider a volume V in the CGS solution (cf. Fig. 1). We divide the volume by a hypothetical plane perpendicular to the Z-axis. The component σ_{zx} of the stress tensor is now given through the following definition:

$$\sigma_{zx} = \overline{S_{zx}}/A. \tag{48}$$

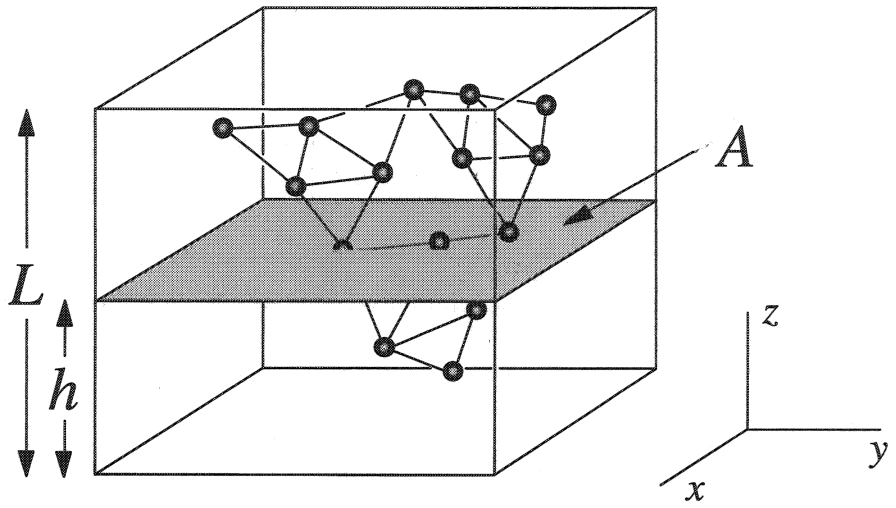

Figure 1: Microscopic derivation of the stress-tensor of a solution of GGSs (see text for details)

Here S_{zx} denotes the force which the upper part of the volume exerts on the lower part through the plane A; the dash denotes the configurational average with respect to the monomers. If we neglect the contribution of the solvent fluid to the force, S_{zx} is given by [19]

$$S_{zx}(h) = \sum_{n,m} F_{mn}^{(x)} \Theta(h - Z_m)\,\Theta(Z_n - h), \tag{49}$$

which depends on the height h of the dividing plane. In Eq. (49) the summations extend over all monomers in the volume V and $F_{mn}^{(x)}$ denotes the X-component of the force $\mathbf{F}_{nm}$ which monomer n exerts on monomer m. Thus σ_{zx} can be written (for short-ranged forces):

$$\sigma_{zx} = \frac{1}{AL}\int_0^L dh\overline{S_{zx}(h)} = \frac{1}{V}\sum_{n,m}\int_0^L dh\overline{F_{mn}^{(x)}\Theta(h - Z_m)\,\Theta(Z_n - h)}. \tag{50}$$

Eq. (50) can be transformed to the simple form [19]

$$\sigma_{zx} = -\frac{c}{N}\sum_{n=1}^{N}\overline{F_n^{(x)} Z_n} \tag{51}$$

where the summation now extends over the monomers of one arbitrary representative of the GGSs, and $\mathbf{F}_n = \sum_n \mathbf{F}_{nm}$ is the total sum of the forces acting on monomer m.

For a GGS $\mathbf{F}_n$ is the sum of all forces exerted by the monomers which are connected to the bead n via a spring (of spring constant $K = 3T/b^2$). Thus

$$F_n^{(x)} = -K \sum_m M_{nm} X_m. \tag{52}$$

Here M_{nm} denotes the generalized Rouse matrix [40] of the GGS which can be constructed as follows. Start with all matrix elements set to zero. Then account for each bond between the monomers n and m by increasing the diagonal components M_{nn} and M_{mm} by $+1$ and M_{nm} and M_{mn} by -1. For a linear structure (*i.e.* a polymer chain) this procedure leads to a tridiagonal matrix which is the well-known Rouse matrix. Inserting Eq. (52) into (51) leads to

$$\sigma_{zx} = \frac{c}{N} \frac{3T}{b^2} \sum_{n,m} \overline{Z_n M_{nm} X_m}. \tag{53}$$

Now we switch from the $\{\mathbf{R}_n\}$ coordinates to the normal coordinates $\{\mathbf{R}(p)\}$; these two sets are related to each other through, say for the X-component, $X_n = 2 \sum_p X(p) m_n(p)$. Here $m_n(p)$ denotes the nth component of the pth eigenvector of M, corresponding to the eigenvalue λ_p, *i.e.* $\sum_k M_{nk} m_k(p) = \lambda_p m_n(p)$. We normalize $m_n(p)$ as follows: $\sum_n m_n(p) m_n(q) = 2\delta_{pq}/N$. In terms of these normal coordinates Eq. (53) takes the following form:

$$\sigma_{zx} = \frac{c}{N} \frac{3T}{b^2} \sum_p 2N\lambda_p \overline{X(p) Z(p)} \tag{54}$$

Now let us perform a steplike deformation of the GGS solution at $t = 0$, *i.e.*, let the strain tensor be of the form $\varepsilon_{zx}(t) = \Theta(t)$ (see Ref. [39] for a definition of $\varepsilon_{\alpha\beta}$). Then for $t \geq 0$ the relaxation of the stress σ_{zx} is given by the relaxation modulus $G(t)$. Microscopically, the step deformation means that at $t = 0$ each monomer gets displaced by $Z_n(t = 0)$ in the X-direction. Solving the corresponding Langevin equation (see Ref. [25]) it follows that

$$\overline{X(p,t) Z(p,t)} = \frac{T}{2KN\lambda_p} \exp\left(-2K\lambda_p t/\zeta\right) \tag{55}$$

Thus we find for the relaxation modulus of the CGS solution

$$G(t) = \frac{c}{N} T \sum_p \exp\left(-2K\lambda_p t/\zeta\right) \tag{56}$$

Now the behavior for $t < \tau_G$ can be calculated by converting the sum over p into an integral; this leads to

$$G(t) \cong cT \int_0^\infty d\lambda n(\lambda) \exp(-2K\lambda t/\zeta) \cong cT (\zeta/K)^{d_s/2} t^{-d_s/2}. \quad (57)$$

Here $n(\lambda)$ denotes the spectral density of the eigenvalues of M which for $N^{-2/d_s} < \lambda < 1$ is given by $n(\lambda) \cong n^{d_s/2-1}$, cf. Refs. [23,24]. This result was also found by Cates [41].

For an arbitrary strain history $\varepsilon_{zx}(t)$ the stress $\sigma_{zx}(t)$ is given by the causal convolution

$$\sigma_{zx}(t) = \int_{-\infty}^t d\tau G(t-\tau) \frac{d\varepsilon_{zx}(\tau)}{d\tau}. \quad (58)$$

Using Eq. (57) we find the following fractional stress-strain relationship

$$\sigma_{zx}(t) \cong cT (\zeta/K)^{d_s/2} \frac{d^{d_s/2}\varepsilon_{zx}(t)}{dt^{d_s/2}}. \quad (59)$$

3 Applications to Rheological Constitutive Equations

In the last subsection we have shown how the (fractional) stress-strain relationship, Eq. (59) which describes the macroscopic mechanical properties of GGS solutions emerges from the microscopic dynamics of its constituents. The viewpoint of the current section is different: We attempt to find stress-strain relationships which properly *describe* the rheological properties of wide classes of materials. This phenomenological approach will lead us to rheological constitutive equations (RCE) with fractional derivatives. We note that the description of viscoelastic properties of materials by means of fractional calculus has a long history, which is discussed in detail in Ref. [42].

In the next section we describe the classical approach to viscoelasticity by exemplarily introducing the Maxwell model; furthermore we show that this model may be generalised by simply replacing the ordinary derivatives in its RCE by fractional ones. A word of caution is here necessary; arbitrarily replacing in RCE ordinary derivatives by fractional ones has its pitfalls: as a general procedure it can easily lead to physically meaningless results: It is therefore indispensable to have procedures at hand which automatically guarantee that the resulting fractional expressions are physically correct. To achieve this we start from mechanical analogues, a topic which is the subject of investigation

of Sec. 3.2. Using this method large classes of physically meaningful fractional RCEs can be formulated; in Sec. 3.3 we present a list of RCEs based on fractional elements (FEs) for which all important material functions are known in analytical, closed form. Finally, we demonstrate in Sec. 3.4 the usefulness of fractional RCEs, by applying them to several viscoelastic materials, by determining the corresponding response functions and by comparing these to the experimental results.

3.1 Viscoelasticity: Classical Approach and its Fractional Generalization

The usual phenomenological viscoelastic models are based on springs and dashpots [38,39]. The springs, Fig. 2(a), obey Hooke's law

$$\sigma(t) = E\varepsilon(t) \tag{60}$$

whereas for dashpots, Fig. 2(b), Newton's law holds:

$$\sigma(t) = \eta \frac{d\varepsilon\,(t)}{dt}. \tag{61}$$

Here σ and ε are the stress and strain of the corresponding mechanical model and E and η denote the spring constant and the viscosity. Now the stress σ and the strain ε in Eqs. (60) and (61) may be interpreted as being components of the stress and strain tensors, say σ_{zx} and ε_{zx} of a macroscopic object. Then Hooke's law represents the RCE of an ideal solid, whereas Newton's law corresponds to an ideal fluid.

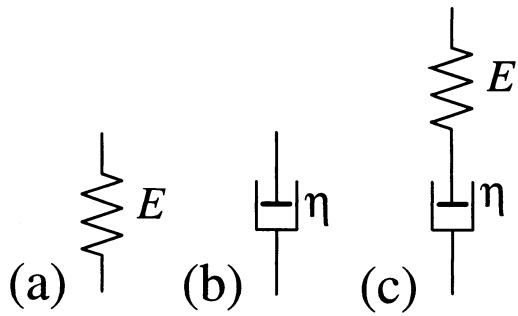

Figure 2: (a) The spring and (b) the dashpot are the structural parts of ordinary viscoelastic models. An example is (c) the Maxwell model where the spring and the dashpot are arranged in a sequential manner.

In general, real objects (such as macromolecular materials) show a behavior which combines characteristic features of solids and liquids, *i.e.* they are viscoelastic. In order to derive RCEs for viscoelastic materials one often starts from mechanical arrangements which combine a small number of springs and dashpots in suitable ways; by this method one arrives at several standard viscoelastic models. To give an example, let us combine a spring and a dashpot in series (Fig. 2(c)); this leads to the classical Maxwell model [38,39]. Here the two components obey the stress-strain relations $\sigma_1(t) = E\varepsilon_1(t)$ for the spring and $\sigma_2(t) = \eta d\varepsilon_2(t)/dt$ for the dashpot. Due to the sequential construction of the arrangement the stresses are equal for both structural parts, $\sigma_1 = \sigma_2 = \sigma$ whereas the strains add, $\varepsilon_1 + \varepsilon_2 = \varepsilon$. This leads to

$$\sigma(t) + \tau \frac{d\sigma(t)}{dt} = \tau E \frac{d\varepsilon(t)}{dt} \tag{62}$$

which is the RCE of the ordinary Maxwell model.

The *relaxation modulus* $G(t)$, *i.e.*, the stress response of the system to a shear jump $\varepsilon(t) = \Theta(t)$ follows from Eq. (62) to be exponential, namely

$$G(t) = E \exp(-t/\tau)\,\Theta(t)\,. \tag{63}$$

Thus the Maxwell model leads to an exponential stress decay; real materials, however, show in many cases a more general behavior. This is also the case for microscopic models of polymer dynamics, such as the Rouse model: In Sec. 2.5 we showed that – as a result of the linear superposition of normal modes – the stress relaxation is non-exponential, obeying an algebraic decay, namely $G(t) \propto t^{-\gamma}$ (with $0 < \gamma < 1$; cf. Eq. (57)). Such algebraic patterns occur for wide classes of polymeric materials over many decades in time. It is thus natural to ask how the classical viscoelastic models have to be extended in order to be able to reproduce such decay patterns.

A direct approach to create fractional RCE is to replace the regular derivatives of ordinary RCE by fractional derivatives ($d^{\gamma_i}/dt^{\gamma_i}$) of non-integer order ($0 < \gamma_i < 1$) [43]. In the case of the Maxwell model, Eq. (62), this procedure leads to

$$\sigma(t) + \tau^{\gamma_1} \frac{d^{\gamma_1}\sigma(t)}{dt^{\gamma_1}} = \tau^{\gamma_2} E \frac{d^{\gamma_2}\varepsilon(t)}{dt^{\gamma_2}} \tag{64}$$

with $0 < \gamma_1 < 1$ and $0 < \gamma_2 < 1$. The relaxation modulus of this generalised Maxwell model can be calculated analytically using different methods [43]– [45]. Interestingly, Eq. (64) is physically meaningful only for γ_i-values in a restricted range: An analysis of the RCE shows (see Sec. 3.3) that $G(t)$ behaves like $t^{\gamma_1-\gamma_2}$ for short times, $t \ll \tau$. Thus for $\gamma_1 > \gamma_2$ the relaxation function

increases, which is in general not reasonable [43,44], and one has to require that $\gamma_1 \leq \gamma_2$.

This example shows that constructing fractional RCEs through direct replacement ($d/dt \rightarrow d^{\gamma_i}/dt^{\gamma_i}$) is unsatisfactory: Only after an in depth analysis of the solutions of such fractional RCE can one decide, *a posteriori*, whether the solutions are physically meaningful or not. In the next section we describe another method which is easy to implement and which has the big advantage that it guarantees automatically that the fractional RCEs obtained through it are physically correct.

3.2 Mechanical Analogues to Fractional Rheological Equations

Let us start by constructing a simple RCE which is physically sound. We assume a given, linear system, which displays the following response function:

$$G(t) = \frac{E}{\Gamma(1-\gamma)} \left(\frac{t}{\tau}\right)^{-\gamma} \tag{65}$$

with $0 < \gamma < 1$. We already know a physical model which leads to such a decay pattern, namely solutions made of Rouse-type GGS, cf. Eq. (57). By comparing Eq. (65) with Eqs. (3) and (8) we obtain the fractional RCE corresponding to this state:

$$\sigma(t) = E\tau^{\gamma} \frac{d^{\gamma}\varepsilon(t)}{dt^{\gamma}}. \tag{66}$$

Note that Eq. (66) is an interpolation between Hookes law, Eq. (60) ($\gamma = 0$) and Newton's law, Eq. (61) ($\gamma = 1$).

Schiessel and Blumen [46,47], Schiessel *et al* [45,48], Heymans and Bauwens [49] and Heymans [50] have demonstrated that the fractional relation, Eq. (66), can be realized physically through hierarchical arrangements of springs and dashpots, such as ladders, trees and fractal networks. In the limit of an infinite number of constitutive elements these arrangements obey Eq. (66). We sketch here two examples, namely the ladder structure introduced in Ref. [46] and the fractal arrangement discussed in Ref. [47]. In Fig. 3 we display a ladder-like structure consisting of springs (with spring constants E_0, E_1, E_2,...) along one of the struts and dashpots (with viscosities η_0, η_1, η_2,...) along the rungs of the ladder. We have shown in Ref. [46] that for equal spring constants and viscosities, *i.e.* for $E = E_0 = E_1 = ...$ and $\eta = \eta_0 = \eta_1 = ...$, this arrangement obeys Eq. (66) with $\tau = \eta/E$ and $\gamma = 1/2$. Moreover, the sequential structure of Fig. 3 also allows to attain other γ-values, by choosing E_k and η_k with k

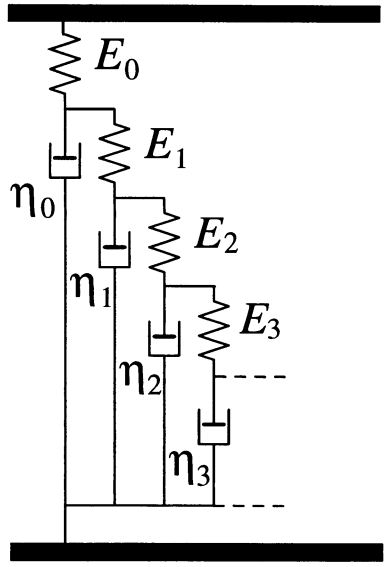

Figure 3: Spring-dashpot ladder: A sequential realisation of the fractional element.

in a suitable way. Thus it suffices to let the spring constants and viscosities obey [46]

$$E_k \propto k^{1-2\gamma} \text{ and } \eta_k \propto k^{1-2\gamma} \tag{67}$$

in order to have an arrangement which obeys Eq. (66) with $0 < \gamma < 1$.

In Ref. [51] we have shown that the linear Rouse-model and the simple ladder model (all E and η are equal, $\gamma = 1/2$) are closely related. Indeed, the similarity between Eqs. (30) and (66) is not accidental. The physical situation of the Rouse chain is, in fact, very close to the ladder arrangement in Fig. 3: In both cases one pulls at the end of an object which is connected by springs and exposed to a velocity dependent friction.

Here an interesting question arises, namely whether it is possible to construct spring-dashpot arrangements which correspond to the GGSs discussed in Sec. 2.2. Such fractals were indeed analysed by us in Ref. [47]. As an example consider the Sierpinski-like structure depicted in Fig. 4. Such a model obeys $\gamma = 1 - d_s/2$ (cf. Ref. [47]), *i.e.*, the connectivity of the network determines the order of derivation in Eq. (66).

As a next step we introduce now the concept of *fractional element* (FE); we define a FE as being a mechanical arrangement which obeys Eq. (66) (without

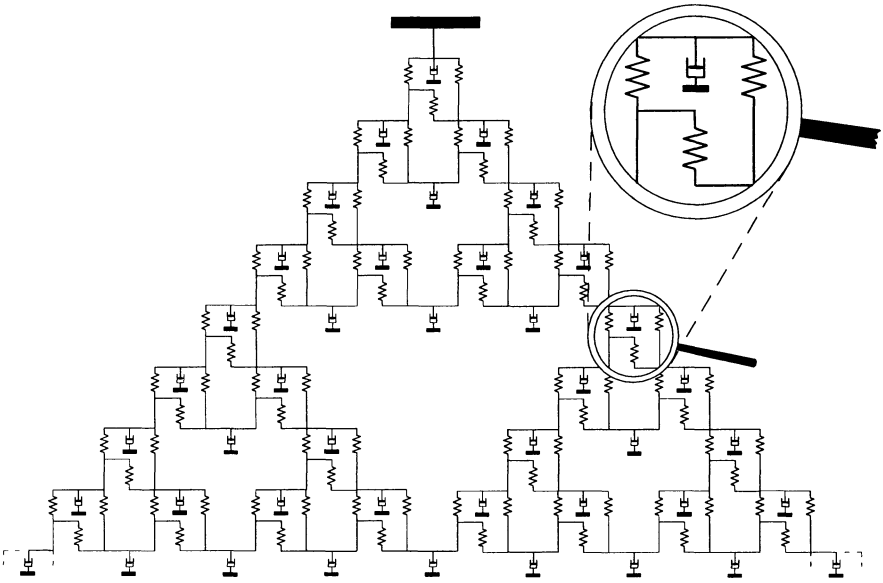

Figure 4: Sierpinski-like network of springs and dashpots: Here the connectivity of the structure controls its rheological properties.

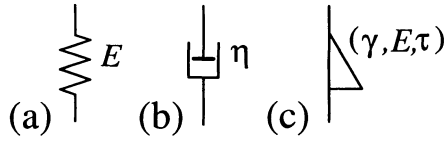

Figure 5: Single elements: (a) elastic, (b) viscous and (c) fractional element.

caring about its specific inner structure). A FE is specified by a triple (γ, E, τ) and we symbolize it by a triangle, as shown in Fig. 5(c), where also its classical counterparts, the spring and the dashpot, are depicted. In the following we will treat a FE on the same footing as a spring or a dashpot, namely as being an elementary building block of mechanical arrangements.

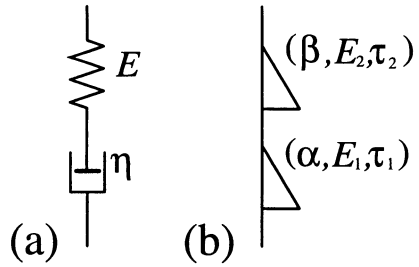

Figure 6: (a) The Maxwell model and (b) its fractional generalisation.

Now we have a method at hand to carry out a proper generalization of the classical Maxwell model, which we depict again in Fig. 6(a): We simply replace the two classical elements by FEs with the parameters (α, E_1, τ_1) and (β, E_2, τ_2), cf. Fig. 6(b). The FEs obey the stress-strain relations $\sigma_1(t) = E_1 \tau_1^\alpha d^\alpha \varepsilon_1(t)/dt^\alpha$ and $\sigma_2(t) = E_2 \tau_2^\beta d^\beta \varepsilon_2(t)/dt^\beta$. Due to the sequential construction of the arrangement one finds

$$\sigma(t) + \frac{E_1 \tau_1^\alpha}{E_2 \tau_2^\beta} \frac{d^{\alpha-\beta}\sigma(t)}{dt^{\alpha-\beta}} = E_1 \tau_1^\alpha \frac{d^\alpha \varepsilon(t)}{dt^\alpha}. \tag{68}$$

Let us assume without loss of generality $\alpha > \beta$. Equation (68) can be further simplified by setting

$$\tau = \left(E_1 \tau_1^\alpha / E_2 \tau_2^\beta\right)^{1/(\alpha-\beta)} \quad \text{and} \quad E = E_1 \left(\tau_1/\tau\right)^\alpha. \tag{69}$$

This leads to

$$\sigma(t) + \tau^{\alpha-\beta} \frac{d^{\alpha-\beta}\sigma(t)}{dt^{\alpha-\beta}} = E\tau^\alpha \frac{d^\alpha \varepsilon(t)}{dt^\alpha}. \tag{70}$$

which is the RCE of the fractional Maxwell model [43,45,52]. Now compare Eq. (70) with Eq. (64): The parameter γ_1 has to be identified with $\alpha - \beta$ and γ_2 with α. Note that due to the mechanical construction, our fractional Maxwell model obeys *automatically* $\gamma_1 \leq \gamma_2$. A further advantage of our method is

that the schematic representation of the model, Fig. 6(b), is much easier to grasp than the corresponding RCE, Eq. (70). This advantage increases with the number of FEs involved, as the next examples will show.

3.3 Overview over Exactly Solvable Fractional Models

Here we list FE based models for which all relevant response functions are known analytically, namely the relaxation modulus, the creep compliance, the complex modulus and the complex compliance. Now, the relaxation modulus $G(t)$ was already introduced. The *shear creep compliance* $J(t)$ is the response of the strain to the shear $\sigma(t) = \Theta(t)$. $G(t)$ and $J(t)$ are the so-called step response functions. On the other hand, the so-called harmonic response functions are defined as follows: The *complex shear modulus* $G^*(\omega)$ describes the response of the stress to a harmonic strain excitation $\varepsilon(t) = \exp(i\omega t)$, *i.e.* $\sigma(t) = G^*(\omega)\exp(i\omega t)$; from $G^*(\omega)$ the *storage* and the *loss moduli*, $G'(\omega) = \mathrm{Re}(G^*(\omega))$ and $G''(\omega) = \mathrm{Im}(G^*(\omega))$, follow. *The complex shear compliance* $J^*(\omega)$ is the response of the strain to a harmonic stress excitation $\sigma(t) = \exp(i\omega t)$; the *storage* and *loss compliances* are defined by $J'(\omega) = \mathrm{Re}(J^*(\omega))$ and $J''(\omega) = -\mathrm{Im}(J^*(\omega))$.

In the context of fractional RCEs, the dynamical response functions are extremely useful: (*i*) In many rheological experiments they are measured directly (cf., for instance, Ref. [42] and subsection 3.4) and (*ii*) for a given fractional RCE they can be easily derived. This can be inferred from the behavior of fractional derivatives under Fourier transformation. The Fourier transform

$$\mathcal{F}\{f(t)\} = \widetilde{f}(\omega) = \int_{-\infty}^{\infty} dt f(t)\exp(-i\omega t) \tag{71}$$

turns the operation d^γ/dt^γ into a simple multiplication [8,9]

$$\mathcal{F}\left\{\frac{d^\gamma f(t)}{dt^\gamma}\right\} = (i\omega)^\gamma \widetilde{f}(\omega). \tag{72}$$

For a given fractional RCE the complex modulus follows directly from

$$G^*(\omega) = \widetilde{\sigma}(\omega)/\widetilde{\varepsilon}(\omega) \tag{73}$$

by using the multiplication rule (72); the complex compliance is then given by $J^*(\omega) = 1/G^*(\omega)$.

Fractional Element

A single FE leads to Eq. (66), which is the simplest fractional RCE. The corresponding mechanical analogue is depicted in Fig. 5(c). The relaxation modulus is given by Eq. (65); the creep compliance follows in analogy to the discussion in Sec. 1, cf. Eq. (11):

$$J(t) = \frac{E^{-1}}{\Gamma(1+\gamma)} \left(\frac{t}{\tau}\right)^{\gamma}. \tag{74}$$

Fourier transforming Eq. (66) leads to $\widetilde{\sigma}(\omega) = E(i\omega\tau)^{\gamma}\widetilde{\varepsilon}(\omega)$, from which

$$G^*(\omega) = E(i\omega\tau)^{\gamma} \tag{75}$$

and

$$J^*(\omega) = E^{-1}(i\omega\tau)^{-\gamma} \tag{76}$$

follow.

Fractional Maxwell Model

In Sec. 3.2 we have already derived the RCE of the fractional Maxwell model, cf. its RCE, Eq. (70), and the mechanical analog, Fig. 6(b). Fourier transforming Eq. (70) and using Eqs. (72) and (73) leads to the complex modulus:

$$G^*(\omega) = \frac{E(i\omega\tau)^{\alpha}}{1+(i\omega\tau)^{\alpha-\beta}}. \tag{77}$$

The complex compliance $J^*(\omega) = 1/G^*(\omega)$ obeys

$$J^*(\omega) = E^{-1}(i\omega\tau)^{-\alpha} + E^{-1}(i\omega\tau)^{-\beta}. \tag{78}$$

Eq. (78) mirrors the fact that for serially arranged elements the compliances of the FEs, Eq. (76), simply add; similarly, the creep compliance is the sum of the compliances of the corresponding two FEs:

$$J(t) = E^{-1}\frac{(t/\tau)^{\alpha}}{\Gamma(1+\alpha)} + E^{-1}\frac{(t/\tau)^{\beta}}{\Gamma(1+\beta)} \tag{79}$$

for all $0 \leq \beta \leq \alpha \leq 1$, a result also reported in Ref. [43] (see also the discussion in Refs. [44,45]).

On the other hand, the determination of the relaxation function $G(t)$ is a difficult task; it can be performed using a power series ansatz [43], a Laplace-Mellin [44] or a Fourier-Mellin method [45]. For the detailed calculations we

refer the interested reader to the original works; here we restrict ourself to the presentation and discussion of the results. The relaxation function is:

$$G(t) = \frac{E}{\alpha - \beta} H_{12}^{11} \left[\frac{t}{\tau} \middle| \begin{matrix} \left(\frac{-\beta}{\alpha-\beta}, \frac{1}{\alpha-\beta}\right) \\ \left(\frac{-\beta}{\alpha-\beta}, \frac{1}{\alpha-\beta}\right) \end{matrix} ; (0,1) \right] \tag{80}$$

or, written differently

$$G(t) = E \left(\frac{t}{\tau}\right)^{-\beta} E_{\alpha-\beta,1-\beta} \left(- \left(\frac{t}{\tau}\right)^{\alpha-\beta} \right). \tag{81}$$

Equations (80) and (81) are two equivalent representations of $G(t)$: Here the $H_{pq}^{nm}(x)$ denote the Fox H-functions [53], which are defined via modified Mellin-Barnes integrals; a detailed discussion of the H-functions can be found in Ref. [45] and in chapter 8 of this book. The $E_{\kappa,\mu}(x)$ stand for the Mittag-Leffler functions [54], which are defined via power series [43,45].

The H-functions may be written in terms of alternating power series, a fact which is convenient for computations. For fractional RCEs we often encounter the form $H_{12}^{11}(x)$ (see Eq. (80) and the other models, discussed below). The power series around $x = 0$ and $x = \infty$ are given by

$$H_{12}^{11} \left[x \middle| \begin{matrix} (a,A) \\ (a,A);(0,1) \end{matrix} \right] = A^{-1} \sum_{k=0}^{\infty} \frac{(-1)^k x^{(k+a)/A}}{\Gamma\left(1 + \frac{k+a}{A}\right)} \tag{82}$$

and

$$H_{12}^{11} \left[x \middle| \begin{matrix} (a,A) \\ (a,A);(0,1) \end{matrix} \right] = A^{-1} \sum_{k=0}^{\infty} \frac{(-1)^k (1/x)^{(k+1-a)/A}}{\Gamma\left(1 - \frac{k+1-a}{A}\right)}. \tag{83}$$

A combination of Eqs. (82) and (83) allows the numerical evaluation of $H_{12}^{11}(x)$ over the complete range of x-values, $x > 0$. Furthermore, from the power series the asymptotic behavior for small and for large arguments can be immediately derived:

$$A\, H_{12}^{11} \left[x \middle| \begin{matrix} (a,A) \\ (a,A);(0,1) \end{matrix} \right] \cong \frac{1}{\Gamma(1 + a/A)} x^{a/A} \tag{84}$$

for $x \ll 1$ and

$$A\, H_{12}^{11} \left[x \middle| \begin{matrix} (a,A) \\ (a,A);(0,1) \end{matrix} \right] \cong \frac{1}{\Gamma\left(1 + \frac{a-1}{A}\right)} x^{\frac{a-1}{A}} \tag{85}$$

for $x \gg 1$.

Now, the behavior of $G(t)$, Eq. (80), for the fractional Maxwell model can be inferred readily. In the parameter range $0 \leq \beta < \alpha < 1$ $G(t)$ obeys at short times, $t \ll \tau$, cf. Eq. (84):

$$G(t) \cong \frac{E}{\Gamma(1-\beta)} \left(\frac{t}{\tau}\right)^{-\beta} \tag{86}$$

whereas at long times ($t \gg \tau$) one has asymptotically, cf. Eq. (85)

$$G(t) \cong \frac{E}{\Gamma(1-\alpha)} \left(\frac{t}{\tau}\right)^{-\alpha}. \tag{87}$$

Equation (80) also includes the special cases $\beta = 0$ and/or $\alpha = 1$; a discussion of these cases can be found in Ref. [45].

Fractional Kelvin-Voigt Model

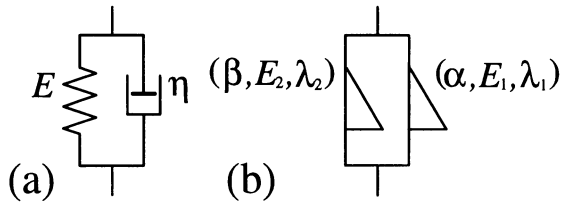

Figure 7: The (a) ordinary Kelvin-Voigt model and (b) its fractional generalisation.

By arranging the spring and the dashpot in parallel one arrives at the standard Kelvin–Voigt model, depicted in Fig. 7(a); its generalisation with two FEs is shown in Fig. 7(b). Because of the parallel construction the individual stresses add. Following the procedure used for the fractional Maxwell model we find the following RCE

$$\sigma(t) = E\tau^{\alpha} \frac{d^{\alpha}\varepsilon(t)}{dt^{\alpha}} + E\tau^{\beta} \frac{d^{\beta}\varepsilon(t)}{dt^{\beta}} \tag{88}$$

where the parameters τ and E are defined as in Eq. (69). By Fourier transforming Eq. (88) we obtain from Eqs. (72) and (73) the complex modulus

$$G^*(\omega) = E(i\omega\tau)^{\alpha} + E(i\omega\tau)^{\beta}, \tag{89}$$

a result that mirrors the additivity of the moduli in parallel arrangements. Similarly, one finds for the relaxation modulus

$$G(t) = E\frac{(t/\tau)^{-\alpha}}{\Gamma(1-\alpha)} + E\frac{(t/\tau)^{-\beta}}{\Gamma(1-\beta)}. \tag{90}$$

On the other hand, the parallel arrangement of the Kelvin-Voigt model causes the complex compliance

$$J^*(\omega) = E^{-1}\frac{(i\omega\tau)^{-\beta}}{1+(i\omega\tau)^{\alpha-\beta}} \tag{91}$$

to be more involved than for the Maxwell model. For the calculation of the function $J(t)$ methods similar to the determination of $G(t)$ for the fractional Maxwell model can be used. This leads to [45]

$$J(t) = \frac{E^{-1}}{\alpha-\beta}H_{12}^{11}\left[\frac{t}{\tau}\middle|\begin{matrix}\left(\frac{\alpha}{\alpha-\beta},\frac{1}{\alpha-\beta}\right)\\ \left(\frac{\alpha}{\alpha-\beta},\frac{1}{\alpha-\beta}\right)\end{matrix};(0,1)\right] \tag{92}$$

or, equivalently, to

$$J(t) = E^{-1}\left(\frac{t}{\tau}\right)^{\alpha}E_{\alpha-\beta,1+\alpha}\left(-\left(\frac{t}{\tau}\right)^{\alpha-\beta}\right). \tag{93}$$

From Eq. (84) we obtain for $t \ll \tau$ the short time behavior of $J(t)$:

$$J(t) \cong \frac{E^{-1}}{\Gamma(1+\alpha)}\left(\frac{t}{\tau}\right)^{\alpha} \tag{94}$$

whereas for $t \gg \tau$ we have asymptotically, cf. Eq. (85):

$$J(t) \cong \frac{E^{-1}}{\Gamma(1+\beta)}\left(\frac{t}{\tau}\right)^{\beta}. \tag{95}$$

A discussion of the special cases $\alpha = 1$ and/or $\beta = 0$ can be found in Ref. [45].

Note the symmetry of the step response functions, $G(t)$ and $J(t)$, in the fractional Maxwell model and in the fractional Kelvin–Voigt model, the two possible arrangements of two FEs. Depending on the construction (sequential for Maxwell or parallel for Kelvin–Voigt) one of these response functions is simply a sum of two algebraic terms (*i.e.* $J(t)$ in the Maxwell model, Eq. (79), and $G(t)$ in the Kelvin–Voigt model, Eq. (90)). Then the other response function is

a Mittag–Leffler function (*i.e.* $G(t)$ for the Maxwell model, Eq. (81), and $J(t)$ for the Kelvin–Voigt model, Eq. (93)). Furthermore, one finds in each case a crossover between two algebraic regimes: For a sum of two algebraic terms this is obvious; in the case of the Mittag–Leffler function this follows from its expression through power series (*vide supra* and Eqs. (84) and (85)).

Fractional Zener Model

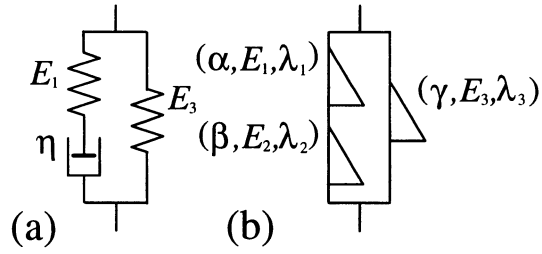

Figure 8: (a) The Zener model and (b) its fractional generalisation.

The so–called Zener or standard solid model [38,39] depicted in Fig. 8(a) involves three elements: It consists of a Maxwell model in parallel with a spring. The most general fractional version of the Zener model is displayed in Fig. 8(b) and consists of three FEs. Without loss of generality, we again require $0 \leq \beta < \alpha \leq 1$ and, of course, $0 \leq \gamma \leq 1$. For this arrangement one finds the following RCE [45]:

$$\sigma(t) + \tau^{\alpha-\beta} \frac{d^{\alpha-\beta}\sigma(t)}{dt^{\alpha-\beta}} = E\tau^{\alpha} \frac{d^{\alpha}\varepsilon(t)}{dt^{\alpha}} + E_0\tau^{\gamma} \frac{d^{\gamma}\varepsilon(t)}{dt^{\gamma}} + E_0\tau^{\gamma+\alpha-\beta} \frac{d^{\gamma+\alpha-\beta}\varepsilon(t)}{dt^{\gamma+\alpha-\beta}}. \tag{96}$$

with τ and E given by Eq. (69) and $E_0 = E_3(\tau_3/\tau)^{\gamma}$. This RCE was given by Tschoegl [39] for the special case $\beta = \gamma = 0$; it was extended to arbitrary $0 \leq \beta < \alpha$ (with $\gamma = 0$) by Friedrich and Braun [55] (cf. also the paper by Metzler et al. [56]).

Using Eqs. (72) and (73) the calculation of the complex modulus $G^*(\omega)$ is straightforward and results in:

$$G^*(\omega) = \frac{E(i\omega\tau)^{\alpha}}{1 + (i\omega\tau)^{\alpha-\beta}} + E_0(i\omega\tau)^{\gamma}. \tag{97}$$

In Eq. (97) the moduli of the Maxwell model, Eq. (77) and of the single FE, Eq. (75), add; this is the direct consequence of the parallel arrangement of Fig. 8(b).

We obtain the resulting relaxation modulus from Eq. (97) by simply adding the moduli of the Maxwell model, Eq. (80), and of the single FE, Eq. (65), *i.e.*

$$G(t) = \frac{E}{\alpha-\beta} H_{12}^{11}\left[\frac{t}{\tau}\middle|\begin{matrix}\left(-\frac{\beta}{\alpha-\beta},\frac{1}{\alpha-\beta}\right)\\ \left(-\frac{\beta}{\alpha-\beta},\frac{1}{\alpha-\beta}\right)\end{matrix};(0,1)\right] + E_0\frac{(t/\tau)^{-\gamma}}{\Gamma(1-\gamma)}. \tag{98}$$

Depending on the parameters, up to four algebraic time regimes may show up. This can be seen by comparing on the RHS of Eq. (98) the generalised Maxwell term (and its power–law behaviors, Eqs. (86) and (87)) with the second term. For instance, in the case $0 \leq \gamma \leq \beta < \alpha$ and for $E \gg E_0$, we find three time regimes

$$G(t) \sim \begin{cases} t^{-\beta} & \text{for} \quad t \ll \tau \\ t^{-\alpha} & \text{for} \quad \tau \ll t \ll \tau_1 \\ t^{-\gamma} & \text{for} \quad \tau_1 \ll t \end{cases} \tag{99}$$

where $\tau_1 \approx (E/E_0)^{1/(\alpha-\gamma)}\,\tau$.

The complex compliance $J^*(\omega) = 1/G^*(\omega)$, *i.e.*

$$J^*(\omega) = \frac{(i\omega\tau)^{-\alpha} + (i\omega\tau)^{-\beta}}{E + E_0(i\omega\tau)^{\gamma-\alpha} + E_0(i\omega\tau)^{\gamma-\beta}} \tag{100}$$

shows a more involved pattern. The creep compliance is known analytically only for the special cases $\gamma = \alpha$ or $\gamma = \beta$, cf. Ref. [45]; we present here the result for $\gamma = \beta$:

$$J(t) = \frac{C_1^{\alpha-2\beta}}{\alpha-\beta}\frac{E}{E_0^2} H_{12}^{11}\left[C_1\frac{t}{\tau}\middle|\begin{matrix}\left(\frac{\alpha}{\alpha-\beta},\frac{1}{\alpha-\beta}\right)\\ \left(\frac{\alpha}{\alpha-\beta},\frac{1}{\alpha-\beta}\right)\end{matrix};(0,1)\right] + \frac{(E+E_0)^{-1}}{\Gamma(1+\beta)}\left(\frac{t}{\tau}\right)^{\beta}. \tag{101}$$

Here we set $C_1 = (E_0/(E+E_0))^{1/(\alpha-\beta)}$. Equation (101) was given in Ref. [55] for the special case $\gamma = \beta = 0$. Note that Eq. (101) expresses $J(t)$ as the sum of two terms which have the same functional dependences as the compliances of the Kelvin–Voigt model, Eq. (92) and of the single FE, Eq. (74), respectively. This similarity follows from the correspondence between the fractional Zener model and the fractional Poynting-Thomson model, which we discuss below.

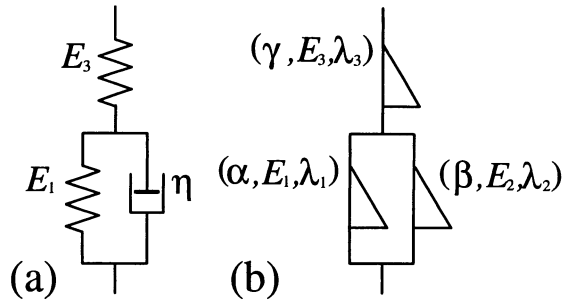

Figure 9: (a) The ordinary and (b) the fractional Poynting-Thomson model.

Fractional Poynting-Thomson Model

The Poynting–Thomson model and its generalisation based on FEs are shown in Figs. 9(a) and (b), respectively. The stress–strain relation of the fractional model obeys

$$\sigma(t) + \frac{E}{E_0}\tau^{\alpha-\gamma}\frac{d^{\alpha-\gamma}\sigma(t)}{dt^{\alpha-\gamma}} + \frac{E}{E_0}\tau^{\beta-\gamma}\frac{d^{\beta-\gamma}\sigma(t)}{dt^{\beta-\gamma}} = E\tau^{\alpha}\frac{d^{\alpha}\varepsilon(t)}{dt^{\alpha}} + E\tau^{\beta}\frac{d^{\beta}\varepsilon(t)}{dt^{\beta}} \tag{102}$$

where τ, E and E_0 are defined as for the fractional Zener model. Due to the serial arrangement of the Poynting–Thomson model we obtain immediately its creep compliance as being the sum of the compliances of its subunits, a Kelvin–Voigt element, Eq. (92) and a FE, Eq. (74):

$$J(t) = \frac{E^{-1}}{\alpha-\beta}H_{12}^{11}\left[\frac{t}{\tau}\,\middle|\,\begin{matrix}\left(\frac{\alpha}{\alpha-\beta},\frac{1}{\alpha-\beta}\right)\\ \left(\frac{\alpha}{\alpha-\beta},\frac{1}{\alpha-\beta}\right)\end{matrix};(0,1)\right] + \frac{E_0^{-1}}{\Gamma(1+\gamma)}\left(\frac{t}{\tau}\right)^{\gamma}. \tag{103}$$

We are able to calculate the relaxation modulus when we restrict ourselves to $\gamma = \alpha$ or to $\gamma = \beta$. Interestingly, the Poynting–Thomson and the Zener model lead then to the same RCEs. In order to distinguish between the material constants of the two models we introduce the superscripts P for Poynting-Thomson and Z for Zener. Thus for $\gamma = \beta$ the RCE of the Poynting–Thomson model, Eq. (102), takes the form

$$\sigma(t) + \frac{E^P\left(\tau^P\right)^{\alpha-\beta}}{E^P+E_0^P}\frac{d^{\alpha-\beta}\sigma(t)}{dt^{\alpha-\beta}} = \frac{E^PE_0^P}{E^P+E_0^P}\left[\left(\tau^P\right)^{\alpha}\frac{d^{\alpha}\varepsilon(t)}{dt^{\alpha}} + \left(\tau^P\right)^{\beta}\frac{d^{\beta}\varepsilon(t)}{dt^{\beta}}\right] \tag{104}$$

whereas the RCE of the Zener model, Eq. (96), for $\gamma = \alpha$ reads:

$$\sigma(t) + \left(\tau^Z\right)^{\alpha-\beta} \frac{d^{\alpha-\beta}\sigma(t)}{dt^{\alpha-\beta}} = \left(E^Z + E_0^Z\right)\left(\tau^Z\right)^{\alpha} \frac{d^{\alpha}\varepsilon(t)}{dt^{\alpha}} + E_0^Z \left(\tau^Z\right)^{\beta} \frac{d^{\beta}\varepsilon(t)}{dt^{\beta}}. \tag{105}$$

By comparing the corresponding terms of Eqs. (104) and (105) we find as transformation rules:

$$\tau^P = \left(\left(E^Z + E_0^Z\right)/E_0^Z\right)^{1/(\alpha-\beta)} \tau^Z, \tag{106}$$

$$E^P = \left(\left(E^Z + E_0^Z\right)/E_0^Z\right)^{(\alpha-2\beta)/(\alpha-\beta)} \left(E_0^Z\right)^2/E^Z \tag{107}$$

and

$$E_0^P = \left(\left(E^Z + E_0^Z\right)/E_0^Z\right)^{(\alpha-2\beta)/(\alpha-\beta)} E_0^Z. \tag{108}$$

These relations connect the two models and are valid for $\gamma = \beta$; for $\gamma = \alpha$ one has simply to exchange α and β in Eqs. (106) to (108), cf. Ref. [45]. Using Eq. (103) and the relations (106) to (108) one recovers Eq. (101) of the fractional Zener model.

This duality can now be invoked to establish the relaxation modulus $G(t)$ in the Poynting–Thomson model; one has only to replace the material constants in the corresponding function of the fractional Zener model, Eq. (98). For $\gamma = \beta$ this leads to [42]

$$G(t) = \frac{C_2^{\alpha-2\beta}}{\alpha-\beta}\frac{E_0^2}{E} H_{12}^{11}\left[\frac{t}{C_2\tau}\,\middle|\,\begin{matrix}\left(\frac{-\beta}{\alpha-\beta},\frac{1}{\alpha-\beta}\right)\\ \left(\frac{-\beta}{\alpha-\beta},\frac{1}{\alpha-\beta}\right)\end{matrix}; (0,1)\right] + \frac{EE_0}{E+E_0}\frac{(t/\tau)^{-\beta}}{\Gamma(1-\beta)} \tag{109}$$

with $C_2 = \left(E/\left(E+E_0\right)\right)^{1/(\alpha-\beta)}$.

3.4 Application to Experimental Data

In Sec. 2 we demonstrated that some special interconnected structures, called GGS, lead directly to power law relaxation, or, equivalently to fractional rheological constitutive equations. The unifying characteristics of different materials displaying such behaviors is the fact that their internal structural units are interconnected and that these units move cooperatively. From this point of view, it is interesting to test the applicability of the derived models for materials whose rheological properties are dominated by their strong connectivity.

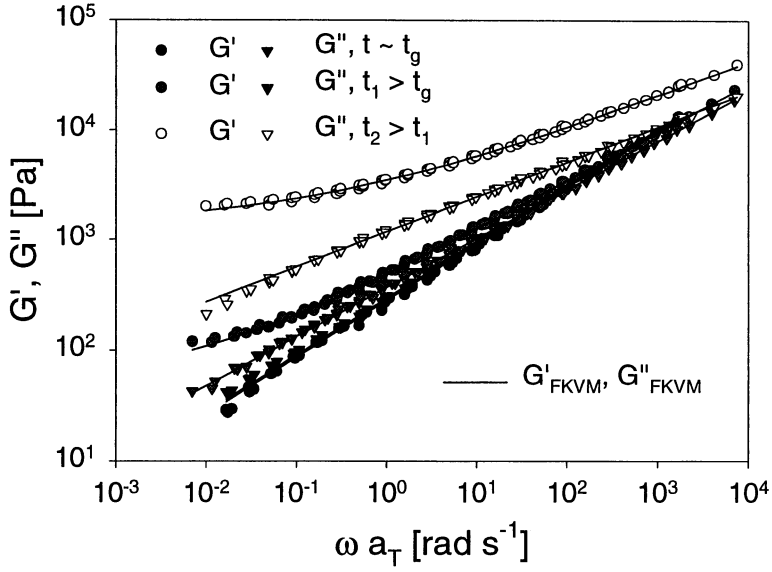

Figure 10: Storage modulus $G'(\omega a_T)$ and loss modulus $G''(\omega a_T)$ of crosslinked polydimethylsiloxane. The shade of the symbols indicates different degrees of crosslinking. The degree depends on the time of the reaction: t_g is the time where the gel point is reached; t_1 and t_2 are later times. The lines represent the fit to the data.

Table 1: Material parameters used in Fig. 10.

time	$S = E\tau^\alpha$, Pa s$^\alpha$	α, –	E_0, Pa
t_g	407	0.51	0
$t_1 > t_g$	572	0.45	52
$t_2 > t_1$	2461	0.31	1340

Gels are obtained either by polymerization of multifunctional monomers or by crosslinking of already formed strands [57]. Such gels correspond closely to GGS. We display in Fig. 10 the dynamical moduli G' and G'' as a function of the reduced frequency, ωa_T, for polydimethylsiloxane (PDMS) at different crosslinking stages [58]. Thus the situation at which the gel structure is attained for the first time is given in black symbols, whereas the situation at two later times is indicated in gray and white. As to be expected, we find at the gelation point in a double-logarithmic plot a linear dependence of both moduli over the whole experimentally accessible domain. This behavior can be fully represented by a single FE, Fig. 5(c). The corresponding expression is Eq. (66). On the other hand, the post-gel regime is characterized by the appearance of an elastic component, which leads to a plateau at low frequencies. In this domain one has to add to the FE a Hookian spring in parallel. This construction is a special case of the Kelvin–Voigt model, Eq. (88), where the order of one of the fractional derivatives is zero, say $\beta = 0$. As also shown in Fig. 10 this model reproduces the data very well; the parameters used are listed in Table 1.

A second example based on interconnected structures is a polymeric matrix (here polypropyleneoxide, PPO) in which a dibenzoylsorbitol (DBS) network is formed [59]. Such networks emerge due to the self-organizing tendency of DBS molecules in certain temperature ranges. Fig. 11 shows such a network. The PPO is the bright background and the grayish threads are fibrils of DBS. The dark points are DBS molecules which are not built in the fibrils and, therefore, form spheres. The interconnection of the fibrils to form a network is the main structural factor leading to the observed power law relaxation in the G' and G'' functions in Fig. 12. The data are best represented by a FE with parameters $\alpha = 0.038$ and $S = E\tau^\alpha = 119000$ Pa s$^\alpha$. In this frequency range the stress in the matrix is always relaxed and the observed behavior is exclusively due to the DBS network.

The third example also pertains to a branched structure [60]. Here a few branches, which are subunits of a syndiotactic polypropylene synthesised with a metallocene catalysator are randomly distributed along the backbone. From

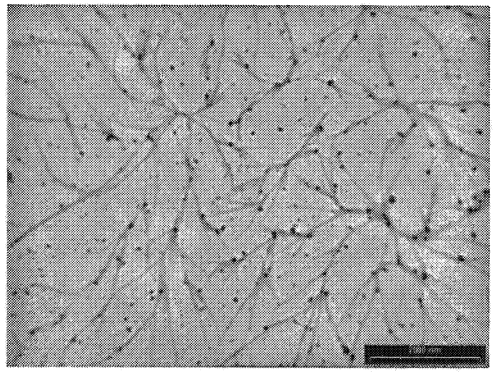

Figure 11: Transmission electron micrograph of a polypropyleneoxide (bright matrix) with dibencoyl sorbitol fibrils (darker network).

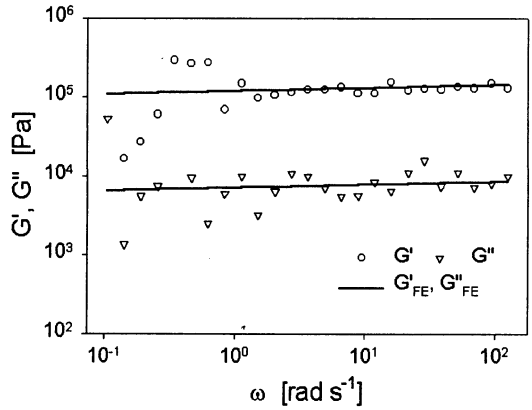

Figure 12: Storage modulus G' (ωa_T) and loss modulus G'' (ωa_T) of polypropyleneoxidcontaining 1 % of dibencoyl sorbitol at $T = 30°C$. The lines represent fits based on a fractional element.

Table 2: Material parameters used in Fig. 14–16.

polymer	τ, s	E, 10^{-5}Pa	α	β
EB64	0.062	3.47	0.69	0.10
EB80	0.048	5.68	0.56	0.06
EB88	0.057	7.24	0.52	0.05

a conformational point of view, such a polymer is classified as "long chain branched" [61]. Such materials flow and, therefore, show a terminal relaxation region, characterized by $G' = \omega^2$ and $G'' = \omega^1$. This behavior is also displayed in Fig. 13. In our case we were able to approach this terminal region experimentally by judiciously combining different techniques (here: dynamic mechanical measurements and creep measurements). On the other hand, in the plateau and in the intermediate ranges we are able to reproduce the observed relaxation by a fractional Maxwell model (FMM). The description of the whole curve by constitutive equations with fractional derivatives is also possible [42,62,63], but beyond the scope of this chapter. The results obtained through the FMM are depicted in Fig. 13 by continuous and dashed lines. Note that the fit of the model to the data is very good in the frequency range considered. For the fit we have taken $E = 4.36 \times 10^5$ Pa, $\tau = 0.242$ s, $\alpha = 0.610$ and $\beta = 0.090$.

Similar features are observed for a poly(ethen-co-1-butene) (EB) copolymer [60]. The storage and loss moduli of three samples with different amounts of ethene incorporation (64, 80 and 88 mol %) are displayed in Figs. 14–16. Only in this range of compositions such a behavior can be observed; we also attribute it to long chain branching. In all three cases the data are well described by the FMM; the corresponding material parameters are given in Table 2.

The fourth example relates to filled polymers. Here we have to use mechanical models composed of three fractional elements. The experimental results are taken from Ref. [64]. Here silicagel nonoparticles are immersed in a polystyrene (PS) matrix. These particles have an average diameter of about 200 nm and are clusters of primary structural units. The primary units are silica spheres of about 15 nm. Such fillers possess an enormous specific interfacial area, which attracts a considerable amount of matrix polymer. This polymeric material can connect the particles, and hence may create a network at quite high particle concentrations. Fig. 17 shows a s.e.m. image of such a compound with 1 vol % of filler. One can recognize the aggregates sitting in the centre of the "nests" formed by the immobilized polymer. The bright rim of the nest is formed from polymer material which disentangles during the process of frac-

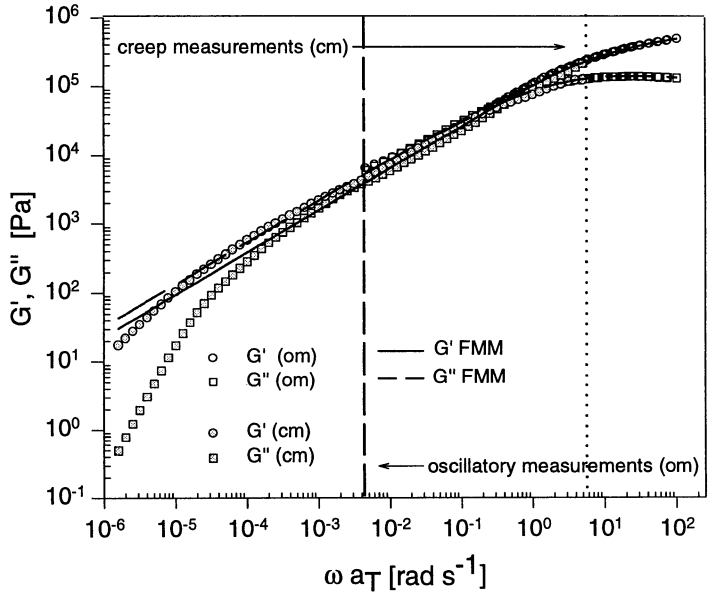

Figure 13: Storage modulus G' (ωa_T) and loss modulus G'' (ωa_T) of syndiotactic polypropylene determined by oscillatory and creep measurements. The vertical lines indicate the frequency range of the corresponding technique of measurements and the reference temperature is $T = 190°C$. The lines represent fits based on the fractional Maxwell element.

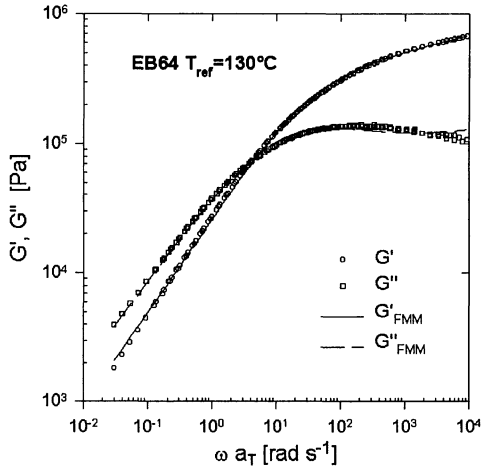

Figure 14: Storage modulus $G'(\omega a_T)$ and loss modulus $G''(\omega a_T)$ of ethene–co–1–butenecopolymer with 64 mol % ethene. The lines represent the fits based on the fractional Maxwell element.

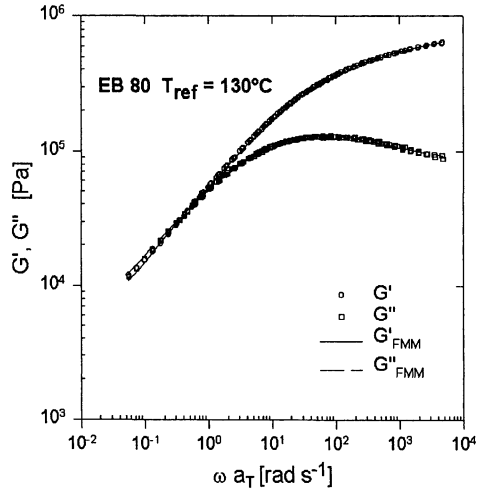

Figure 15: Same as Fig. 14, but with 80 mol % ethene.

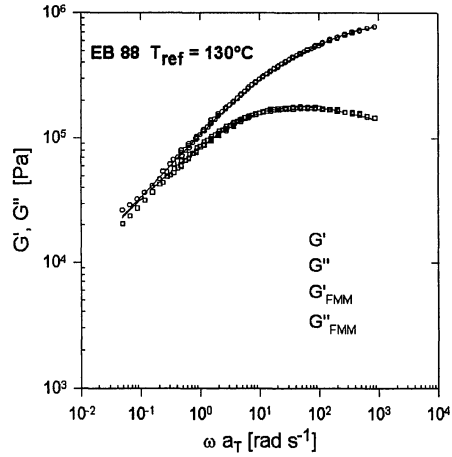

Figure 16: Same as Fig. 14 but with 88 mol % ethene.

Table 3: Material parameters used in Fig. 18.

conc., vol %	t, s	E, 10^{-5}Pa	α	β	E_0, Pa
3	0.087	1.1	0.98	0.20	20
4	0.110	1.51	0.97	0.20	44
5	0.102	1.82	0.93	0.20	532
7	0.089	3.31	0.77	0.17	4460

ture. Fig. 18 shows the storage moduli, G', of polystyrene filled with different amounts of silicagel as a function of the reduced frequency ωa_T. The material functions of these compounds follow a power law in a range intermediate between the plateau region ($\omega a_T > 10$ rad/s) and the low frequency plateau. For modelling purposes we thus have to add a Hookian element in parallel to the two FEs of the FMM. Such a model renders the data very well, as can be seen from the good agreement obtained in Fig. 18. The corresponding material parameters are given in Table 3. We hasten to note that similar results were found by Metzler et al. [56] in describing through RCEs the rheological behavior of filled polymers.

As a last example we display in Fig. 19 the creep behavior of a polypropylene exposed to a constant shear load at room temperature [65]. Under these conditions the material is in the transitional region between the entanglement

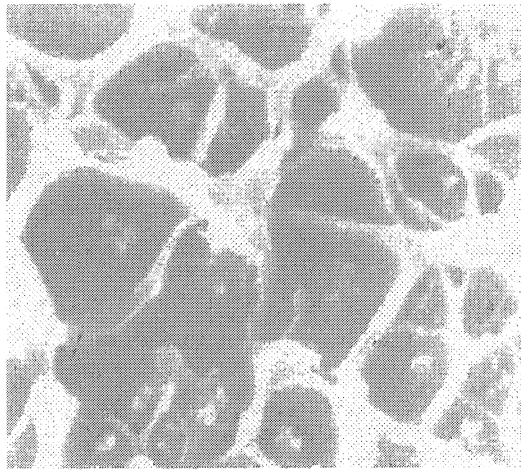

Figure 17: Scanning electron micrograph of a polystyrol filled with 1 vol% silicagel R974.The image represents an area of 1 mm^2.

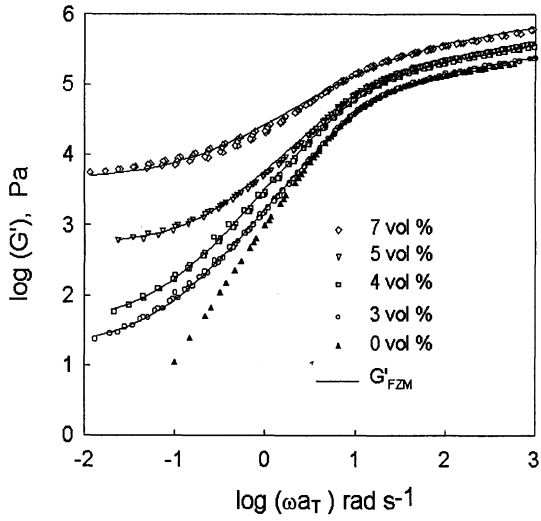

Figure 18: Storage modulus $G'(\omega a_T)$ of silicagel filled polystyrene at $T = 190°C$. The lines represent fits based on the fractional Zener model.

plateau and the glass region. Here only some segments of the polymeric backbone are involved in the relaxational processes. Now, it is well known that such relaxational processes are highly cooperative and, therefore, may lead to a power law behavior for $J(t)$. To describe the experimental results by an appropriate combination of FEs we may view the data as arising as a combination of two distinct patterns. The first pattern is an S-shaped transition from a lower plateau around $J_0 \approx 1.5 \times 10^{-10}$ Pa^{-1} to an upper plateau at $J_1 \approx 4.5 \times 10^{-10}$ Pa^{-1}, whereas the second pattern is a steep increase in the compliance for times longer than 10 s. The S-shaped transition is well represented by the fractional Zener model (FZM), Fig. 8(b). The creep behavior of the FZM is given by Eq. (101) which is valid only under restricted conditions. The presence of the second plateau demands $\gamma = 0$ and we can use Eq. (101) when we set $\beta = 0$. In this case Eq. (101) degenerates to the following expression, which was already suggested elsewhere [55]:

$$J(t) = J_1 - (J_1 - J_0)\, E_{\alpha,1}\left[-(t/\tau_1)^{\alpha}\right], \tag{110}$$

with $J_0 = E^{-1}$ and $J_1 = (E + E_0)^{-1}$. The generalized Mittag-Leffler function $E_{\alpha,1}$ can be calculated based on Padé-approximants [55]. The second pattern can be represented by a simple FE whose creep behavior is given by $J_2 t^{\delta}$. The description of the whole data set is possible by combining these elements in series. Using $J_0 = 1.50 \times 10^{-10}$ Pa^{-1}, $J_1 = 4.21 \times 10^{-10}$ Pa^{-1}, $J_2 = 0.43 \times 10^{-10}$ Pa^{-1}, $\tau = 2.9 \times 10^{-4}$ s, $\alpha = 0.282$ and $\beta = 0.351$ we attain a very good fit. This and all the other results presented here show convincingly that models containing various numbers of FEs allow to reflect quantitatively the rheological behavior of highly interconnected materials.

4 Conclusion

In this chapter we have discussed different applications of fractional calculus to polymer physics and rheology. Fractional expressions come naturally into play for systems which respond algebraically to external perturbations. We show that such situations occur on the microscopic level both for linear polymers (Rouse chains) and for networks (generalized Gaussian structures). Furthermore, we demonstrated rigorously how such behaviors translate into the macroscopic level, which is usually accessible by rheological experiments. This explains why fractional constitutive equations are extremely successful in describing the viscoelastic properties of many polymeric materials. We presented several systems (linear, interconnected and branched structures, gels and filled polymers), for which the fractional expressions lead to excellent fits for the observed relaxation behaviors.

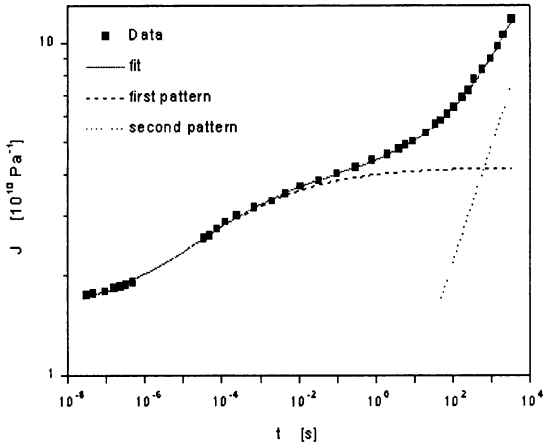

Figure 19: Creep curve of polypropylene at room temperature. The solid line represents a fit using Eq. (111). The dashed lines correspond to the fractional Zener model (left branch, first pattern) and to a simple fractional element (right branch, second pattern).

Acknowledgments

The authors thank Prof. P. Pincus for discussions. The support of the Fonds der Chemischen Industrie and of the DFG (through SFB 428, Graduiertenkolleg, and a stipend to H.S.) are thankfully acknowledged.

References

1. H. Scher and E.W. Montroll, *Phys. Rev.* B **12**, 2455 (1975).
2. H. Schnörer, H. Domes, A. Blumen, and D. Haarer, *Phil. Mag. Lett.* **58**, 101 (1988).
3. R.D. Armstrong and R.A. Burnham, *J. Electroanal. Chem.* **72**, 257 (1976).
4. K.S. Cole and R.H. Cole, *J. Chem. Phys.* **9**, 341 (1941).
5. A.K. Jonscher, *Nature* **267**, 673 (1977).
6. E. Kjartansson, *J. Geophys. Res.* **84**, 4737 (1979).
7. R. Richert and A. Blumen (eds.), *Disorder Effects on Relaxational Processes: Glasses, Polymers, Proteins* (Springer, Berlin, 1994).
8. K.B. Oldham and J. Spanier, *The Fractional Calculus* (Academic Press, New York, 1974).

9. K.S. Miller and R. Ross, *An Introduction to the Fractional Calculus and Fractional Differential Equations* (Wiley, New York, 1993).
10. T.T. Perkins, D.E. Smith, and S. Chu, *Science* **264**, 819 (1994).
11. T.T. Perkins, S.R. Quake, D.E. Smith, and S. Chu, *Science* **264**, 822 (1994).
12. T.T. Perkins, D.E. Smith, R.G. Larson, and S. Chu, *Science* **268**, 83 (1995).
13. D. Wirtz, *Phys. Rev. Lett.* **75**, 2436 (1995).
14. F. Amblard, A.C. Maggs, B. Yurke, A.N. Pergellis, and S. Leibler, *Phys. Rev. Lett.* **77**, 4470 (1996).
15. F. Brochard-Wyart, *Europhys. Lett.* **26**, 511 (1994).
16. F. Brochard-Wyart, *Europhys. Lett.* **30**, 387 (1995).
17. S. Manneville, P. Cluzel, J.-L. Viovy, D. Chatenay, and F. Charon, *Europhys. Lett.* **36**, 413 (1996).
18. P.E. Rouse, *J. Chem. Phys.* **21**, 1272 (1953).
19. M. Doi and S.F. Edwards, *The Theory of Polymer Dynamics* (Claredon Press, Oxford, 1995).
20. H. Schiessel, G. Oshanin, and A. Blumen, *J. Chem. Phys.* **103**, 5070 (1995).
21. H. Schiessel, G. Oshanin, and A. Blumen, *Macromol. Theory Simul.* **5**, 6036 (1996).
22. J.-U. Sommer and A. Blumen, *J. Phys.* A **28**, 6669 (1995).
23. D. Dhar, *J. Math. Phys.* **18**, 577 (1977); S. Alexander and R. Orbach, *J. Physique* **43**, L625 (1982); R. Hilfer and A. Blumen, *J. Phys.* A **17**, L537 (1984).
24. S. Havlin and A. Bunde in *Fractals and Disordered Systems*, eds. A. Bunde and S. Havlin (Springer, Berlin, 1991).
25. H. Schiessel, submitted to *Phys. Rev. E.*
26. P.G. Higgs and J.F. Joanny, *J. Chem. Phys.* **94**, 1543 (1991).
27. A.V. Dobrynin and M. Rubinstein, *Journal de Physique II* **5**, 677 (1995).
28. Y. Kantor and M. Kardar, *Phys. Rev.* E **51**, 1299 (1995).
29. Th. Soddemann, H. Schiessel, and A. Blumen, *Phys. Rev. E* in press.
30. H. Schiessel and A. Blumen, *J. Chem. Phys.* **105**, 4250 (1996).
31. H. Schiessel and A. Blumen, *Macromol. Theory Simul.* **6**, 103 (1997).
32. A.V. Dobrynin, M. Rubinstein, and J.-F. Joanny, *Macromolecules* **30**, 4332 (1997).
33. H. Schiessel and A. Blumen, *J. Chem. Phys.* **104**, 6036 (1996).
34. R.G. Winkler and P. Reineker, *J. Chem. Phys.* **106**, 2841 (1997).
35. D. Loomans, H. Schiessel, and A. Blumen, *J. Chem. Phys.* **107**, 2636 (1997).

36. H. Schiessel, I.M. Sokolov, and A. Blumen, *Phys. Rev. E* **56**, R2390 (1997).
37. G.H. Köhler and A. Blumen in *MATH/CHEM/COMP 1988*, ed. A. Graovac, Elsevier, Amsterdam, *Studies Phys. Theor. Chem.* **63**, 339 (1989).
38. I.M. Ward, *Mechanical Properties of Solid Polymers* (Wiley, Chichester, 1983).
39. N.W. Tschoegl, *The Phenomenological Theory of Linear Viscoelastic Behavior* (Springer, Berlin, 1989).
40. J.-U. Sommer, M. Schulz, and H. Trautenberg, *J. Chem. Phys.* **98**, 7515 (1993); J.-U. Sommer, T.A. Vilgis, and G. Heinrich, *J. Chem. Phys.* **100**, 9181 (1994).
41. M.E. Cates, *J. Physique* **46**, 1059 (1985).
42. Chr. Friedrich, H. Schiessel, and A. Blumen in *Advances in the Flow and Rheology of Non-Newtonian Fluids*, eds. D.A. Siginer, D. De Kee, and R.P. Chhabra (Elsevier, Amsterdam, in press).
43. C. Friedrich, *Rheol. Acta* **30**, 151 (1991).
44. W.G. Glöckle and T.F. Nonnenmacher, *Macromolecules* **24**, 6426 (1991).
45. H. Schiessel, R. Metzler, A. Blumen, and T.F. Nonnenmacher, *J. Phys.* A **28**, 6567 (1995).
46. H. Schiessel and A. Blumen, *J. Phys.* A **26**, 5057 (1993).
47. H. Schiessel and A. Blumen, *Macromolecules* **28**, 4013 (1995).
48. H. Schiessel, P. Alemany, and A. Blumen, *Progr. Colloid Polym. Sci.* **96**, 16 (1994).
49. N. Heymans and J.-C. Bauwens, *Rheol. Acta* **33**, 210 (1994).
50. N. Heymans, *Rheol. Acta* **35**, 508 (1996).
51. H. Schiessel and A. Blumen, *Fractals* **3**, 483 (1995).
52. T.F. Nonnenmacher in *Rheological Modeling: Thermodynamical and Statistical Approaches*, eds. J. Casas-Vazquéz and D. Jou, Springer, Berlin, *Lecture Notes in Physics* **381**, 309 (1989).
53. A.M. Mathai and R.K. Saxena, *The H-function with Applications in Statistics and Other Disciplines* (Wiley Eastern, New-Delhi, 1978).
54. A. Erdélyi (ed.), *Bateman Manuscript Project, Higher Transcendental Functions*, volume III, (McGraw-Hill, New York, 1955).
55. C. Friedrich and H. Braun, *Rheol. Acta* **31**, 309 (1992).
56. R. Metzler, W. Schick, H.-G. Kilian, and T.F. Nonnenmacher, *J. Chem. Phys.* **103**, 7180 (1995).
57. H.H. Winter and M. Mours, *Adv. Polym. Sci* **134**, 165 (1997).
58. F. Chambon and H.H. Winter, *Polym. Bull.* **13**, 499 (1985).
59. K. Fuchs, R.-D. Meier, M. Fahrländer, and Chr. Friedrich, *in prepara-*

tion.
60. A. Eckstein, J. Suhm, O. Meincke, R. Mühlhaupt, and Chr. Friedrich, *in preparation.*
61. J.D. Ferry, *Viscoelastic Properties of Polymers* (John Wiley, New York, 1980).
62. Chr. Friedrich, *Phil. Mag. Letters* **66**, 287 (1992).
63. Chr. Friedrich and H. Braun, *Colloid Polym. Sci.* **272**, 1536 (1994).
64. Chr. Friedrich and H. Dehno in: *Progress and Trends in Rheology IV* (Steinkopfverlag, Darmstadt, 1994), p. 45.
65. B.E. Read, G.D. Dean, and P.E. Tomlins, *Polymer* **29**, 2159 (1988).